



HAL
open science

On the generation and degradation of emerged coral reef terrace sequences: First cosmogenic ^{36}Cl analysis at Cape Laundi, Sumba Island (Indonesia)

Denovan Chauveau, Christine Authemayou, Kevin Pedroja, Stéphane Molliex, Laurent Husson, Denis Scholz, Vincent Godard, Anne-Morwenn Pastier, Gino de Gelder, Sri Yudawati Cahyarini, et al.

► To cite this version:

Denovan Chauveau, Christine Authemayou, Kevin Pedroja, Stéphane Molliex, Laurent Husson, et al.. On the generation and degradation of emerged coral reef terrace sequences: First cosmogenic ^{36}Cl analysis at Cape Laundi, Sumba Island (Indonesia). *Quaternary Science Reviews*, 2021, 269, pp.107144. 10.1016/j.quascirev.2021.107144 . hal-03350633

HAL Id: hal-03350633

<https://normandie-univ.hal.science/hal-03350633v1>

Submitted on 16 Oct 2023

HAL is a multi-disciplinary open access archive for the deposit and dissemination of scientific research documents, whether they are published or not. The documents may come from teaching and research institutions in France or abroad, or from public or private research centers.

L'archive ouverte pluridisciplinaire **HAL**, est destinée au dépôt et à la diffusion de documents scientifiques de niveau recherche, publiés ou non, émanant des établissements d'enseignement et de recherche français ou étrangers, des laboratoires publics ou privés.



Distributed under a Creative Commons Attribution - NonCommercial 4.0 International License

1 **On the generation and degradation of emerged coral reef terrace sequences:**
2 **first cosmogenic ^{36}Cl analysis at Cape Laundi, Sumba Island (Indonesia)**

3
4 Denovan Chauveau^a, Christine Authemayou^a, Kevin Pedoja^b, Stéphane Molliex^a, Laurent
5 Husson^c, Denis Scholz^d, Vincent Godard^e, Anne-Morwenn Pastier^f, Gino de Gelder^c, Sri
6 Yudawati Cahyarini^g, Mary Elliot^h, Michael Weber^d, Lucilla Benedetti^e, Marion Jaud^a, Audrey
7 Boissierⁱ, Vera Christanti Agusta^g, Sonny Aribowo^c, Ann. F. Buddⁱ, Danny Hilman Natawidjaja^g,
8 A.S.T.E.R. Team^e

9
10 ^aLGO, IUEM, CNRS, UMR 6538, Université de Bretagne Occidentale, Plouzané, France

11 ^bM2C, UMR6143, UnivCaen-Normandie, Caen, France

12 ^cISTerre, CNRS, UMR 5275, Université de Grenoble Alpes, Grenoble, France

13 ^dInstitut für Geowissenschaften, Johannes-Gutenberg-Universität Mainz, Mainz, Germany

14 ^eCEREGE, CNRS-IRD, UMR 34, Aix-Marseille Université, Aix-en-Provence, France

15 ^fGFZ German Research Centre for Geosciences, Earth Surface Process Modelling, Potsdam, Germany

16 ^gResearch Center for Geotechnology, Indonesian Institute of Science, LIPI, Bandung, Indonesia

17 ^hLPG, CNRS, UMR 6112, Université de Nantes, Nantes, France

18 ⁱIFREMER, Géosciences Marines, Centre de Brest, Plouzané, France

19 ^jDepartment of Earth and Environmental Sciences, University of Iowa, Iowa City, USA

20

21 **Keywords:** Quaternary; Coral reef terrace; ^{36}Cl cosmogenic isotope; Denudation rate;
22 U-Th series; Coastal erosion; MIS 5; Southeastern Asia.

23

24 **Abbreviations:** Coral Reef Terrace (CRT); Marine Isotope Stage (MIS); Electron Spin
25 Resonance (ESR).

26

27 **Abstract**

28

29 The emerged coral reef terraces sequence at Cape Laundi, on the north coast of
30 Sumba Island (Indonesia), with at least 18 successive strandlines, remains poorly
31 dated in spite of numerous previous data. The age discrepancies within these coral
32 reef terraces (CRTs) were previously explained by their polycyclic nature, triggered by
33 marine erosion and reoccupation of old coral colonies by new ones. This study aims at
34 highlighting these processes, as well as the continental denudation that participates in
35 the partial stripping of the thin superficial coral reef layer overlying the pre-existing
36 surface, exhuming older coral colonies. For this purpose, we use a combined analysis
37 of ^{36}Cl cosmogenic concentrations, new $^{230}\text{Th}/\text{U}$ ages, and previous dating in order to
38 quantify denudation rates affecting the sequence and to highlight the role of marine
39 erosion in reworking the lowest CRT surface. Our results demonstrate that 1) the
40 lowermost CRT is composite, i.e., formed by different reefal limestone units
41 constructed and eroded during successive highstands of the last interglacial, 2)
42 following the last deglaciation, this CRT has been subjected again to coastal erosion
43 and reoccupation during the Mid Holocene highstand, 3) its distal edge is affected by
44 the current marine erosion and shows denudation rates higher by one to two orders of
45 magnitude (from 279 ± 0.4 to 581 ± 0.4 mm ka⁻¹) than the continental denudation
46 values of higher CRTs (14.7 ± 8.3 mm ka⁻¹ on average), 4) at the scale of a single CRT
47 surface, variations in continental denudation rates are caused by epikarstification
48 roughness, 5) the distal edges have the highest continental denudation rate due to
49 diffusion and regressive erosion produced by the runoff occurring along the steep
50 downward cliff.

51

52 **1. Introduction**

53

54 Sumba is an actively rising island in Indonesia where an emerged coral reef terraces
55 sequence records the progressive emergence of the island. The sequence at Cape
56 Laundi, on the north coast of the island, reaches ~470 m in elevation and includes at
57 least 18 successive coral reef terraces (CRTs). This sequence has a well-preserved
58 and potentially valuable record of Quaternary sea level, paleoclimate and tectonics, for
59 which dating of the CRTs is crucial. The previous studies of this CRTs sequence
60 (Pirazzoli et al., 1991; 1993; Bard et al., 1996) have identified significant temporal
61 discrepancies within the CRTs, i.e., different ages of corals within the same CRT and
62 similar ages of corals on several CRTs. Pirazzoli et al. (1991; 1993) and Bard et al.
63 (1996) proposed that the CRTs have a polycyclic nature in order to explain age
64 diachronism (Fig. 1). Pirazzoli et al., (1993) suggested that marine erosion can reshape
65 the CRT surface and promote the bioconstruction of a new coral-colony on an older
66 one during sea level highstands (Fig. 1A). Bard et al. (1996) indicated that a decrease
67 in the rate of uplift to a low rate would in recurrent similar relative sea levels, causing
68 several phases of reef development on a pre-existing surface (Fig. 1B). The role of
69 marine erosion on the morphogenesis of CRTs has been discussed since a long time
70 (e.g., Chappell, 1974; Hearty et al., 2008). Despite the persistence in recent
71 publications of a simplistic definition of CRTs as constructive marine terraces; it is now
72 clearly accepted in many syntheses that a CRT surface results from the combination
73 of bioconstruction, erosion at sea level and accumulation of the eroded sediments
74 (Pirazzoli, 2005; Cabioch, 2011; Murray-Wallace and Woodroffe, 2014; Pedoja et al.,
75 2018; Pastier et al., 2019).

76

77 Apart from the role of marine erosion and bioconstruction reoccupation, what is the
78 role of continental denudation in age diachronism on the same CRT? On polycyclic

79 CRT, continental denudation could partially strip the thin superficial layer of a young
80 fossil coral reef and exhume older corals in several places (Fig. 1C). Since the
81 stratigraphy of the CRTs on Sumba is not described and is difficult to observe in the
82 canyons that incise them, and since the preservation of paleo-soils is unlikely in the
83 polycyclic CRTs by their subsequent marine abrasion during a new transgression, we
84 have chosen to combine the cosmogenic ^{36}Cl method (e.g., Lal, 1988; 1991; Bierman,
85 1994), new $^{230}\text{Th}/\text{U}$ dating and previous dating to highlight the processes of marine
86 erosion, reoccupation and continental denudation affecting the CRTs of Cape Laundi.
87 The ^{36}Cl method has already been carried out on CRTs in Barbados, resulting in
88 quantification of the continental denudation rate (Lal et al., 2005).

89

90 In this study, we measured the cosmogenic ^{36}Cl isotopes concentration of 34 *in situ*
91 surface samples collected from the oldest CRT to the current reef shelf and took
92 several samples on each CRT from the inner edge to the lower cliff in order to detect
93 variation of continental denudation on them (Figs. 1C; 2). Moreover, we analyzed the
94 ^{36}Cl concentration in a 2.5 ± 0.1 m deep core of the lowermost CRT to attempt to (1)
95 constrain its exposure time to cosmic rays (i.e., the age at which it emerged) if the
96 concentration of ^{36}Cl decreases exponentially at depth (e.g., Braucher et al., 2011), or
97 (2) to detect several exposure phases (i.e., reoccupation stages) by ^{36}Cl concentration
98 peaks at depth (Figs. 1A; 1B). We conducted $^{230}\text{Th}/\text{U}$ dating of two coral colonies in
99 growth position collected on the Holocene landform and used these $^{230}\text{Th}/\text{U}$ ages to
100 calculate a coastal denudation rate from the ^{36}Cl concentrations of samples taken from
101 the top of the active Holocene sea cliff. We discuss our results in terms of 1) their
102 comparison with global trends, as well as 2) continental denudation rates of carbonates

103 and their heterogeneity, and 3) the influence of marine erosion and constructive
104 reoccupation components on CRT morphogenesis.

105

106 **2. Background**

107 **2.1. Emerged coral reef terrace sequences**

108

109 Morphologically, a CRT is an expanse of reefal limestone with a surface that is flat or
110 slightly sloping seawards, limited by a change in slope seaward and landward.
111 Seaward, the change in slope (i.e., a distal edge associated with a more or less steep
112 cliff; Fig. 2), is usually described as the paleo reef crest (e.g., Pirazzoli et al., 1991;
113 Rovere et al., 2016). Landward, at the inner edge, a CRT is characterized by a break
114 in slope, sometimes interpreted as a shoreline angle suggesting the erosional sea cliff
115 nature (e.g., Speed and Cheng, 2004; Pedoja et al., 2018). This break in slope provides
116 a rather good marker for relative sea level, usually associated with the sea level
117 highstands of former interglacial stages (e.g., Pirazzoli et al., 1993; Bard et al., 1996;
118 Pedoja et al., 2018).

119

120 CRTs are geomorphologic plane surfaces encountered in the tropical zones and are a
121 type of marine terraces in the broadest sense of the term (Schwartz, 2006; Murray-
122 Wallace and Woodroffe, 2014; Pedoja et al., 2018). When the global sea level falls too
123 rapidly and/or the reef is lifted by tectonic movements or glacial isostatic adjustment, it
124 emerges, dies, and fossilizes, forming a CRT. The joint effects of sea level oscillations
125 and tectonic uplift can result in the generation of a CRTs sequence with a staircase
126 geometry (Fig. 2) (e.g., Chappell, 1974; Pirazzoli, 2005). Since the 19th century, such
127 sequences have been described in the Caribbean province (Haiti, Cuba, Barbados;

128 e.g., Crosby, 1883; Simms, 2021; Thompson and Creveling, 2021), in the Indo-Pacific
129 province (Indonesia, Papua New Guinea, Japan, Fiji, Philippine, and other islands or
130 archipelagos; e.g., Darwin, 1842; Daly, 1915; Pirazzoli et al, 1993; Pedoja et al, 2018),
131 as well as alongshore the Red Sea (Scholz et al., 2004; Murray-Wallace and
132 Woodroffe, 2014; Pedoja et al., 2011; 2014; Obert et al., 2019).

133

134 The stratigraphy and morphology of a CRT, as well as these of a sequence, result from
135 interactions between the vertical land motion, absolute and relative sea level
136 variations, slope of the foundations, erosion processes (either mechanical or chemical
137 and marine or continental in origin), reef bioconstruction, subsequent accumulation of
138 eroded sediments and reef reoccupation (e.g., Pirazzoli, 2005; Cabioch, 2011; Husson
139 et al., 2018; Pedoja et al., 2018; Pastier et al., 2019). Rates of reef growth, marine
140 erosion and sedimentation may vary spatially due to a change in shoreline direction
141 (e.g., from a bay to a cape), resulting in a modification in the final geometry of the
142 sequence (Fig. 2). Thus, one CRT with a continuous high fossil sea cliff (>10 m; CRT
143 I in figure 2) can include numerous secondary or intermediate CRTs (CRTs I₁ and I₂ in
144 figure 2) with or without low (<10 m), eroded, fossil sea cliffs and various reefal
145 limestone units (Fig. 2) (Hantoro et al., 1989; Pirazzoli et al., 1993; Speed and Cheng,
146 2004). Geomorphologically, these compound CRTs are named main CRTs (e.g.,
147 Pirazzoli et al., 1993). These main CRTs, sometimes morphologically forming a single
148 CRT (CRT I in figure 2), may contain coral colonies sampled in growth position on their
149 surface providing ages associated with different Marine Isotope Stage (MIS) (the
150 different reefal limestone units on CRT I in figure 2) (e.g., Pirazzoli et al., 1993; Bard
151 et al., 1996). When such a diachronism is observed, these CRTs are named composite
152 CRTs (e.g., Kindler et al., 2007).

153

154 **2.2. Sumba Island**

155 **2.2.1. Tectonic and geologic setting**

156

157 Sumba is a 220 km-long and 65 km-wide island located in the lesser Sunda
158 Archipelago, Indonesia. It is located near the transition from oceanic subduction in the
159 West, along the Java trench, to the collision of the Banda arc with the continental
160 Indian-Australian plate in the East (Fig. 3) (Hinschberger et al., 2005). The Cretaceous
161 to Oligocene crystalline basement is almost entirely covered by Miocene and Pliocene
162 deposits (Abdullah et al., 2000). The Miocene rocks consist of carbonate platform
163 deposits to the west that evolve eastward into deep basin deposits (Von der Borch et
164 al., 1983; Van der Werff et al., 1995). Since the late Miocene/Pliocene, the
165 convergence between the Eurasian and Indian-Australian plates has been driving
166 shortening and uplift in the fore-arc domain (e.g., Harris, 1991; Fortuin et al., 1997;
167 Haig, 2012; Tate et al., 2014). In Sumba island, the Quaternary uplift is recorded by a
168 ~350 km long CRTs sequence (e.g., Pirazzoli et al., 1991; Bard et al., 1996). The
169 Sumba sequence is nearly continuous, interrupted only locally by large rivers. It spans
170 approximately two-thirds of the island's shores, mostly along its northern coast and the
171 eastern and western tips of the island (Hantoro, 1992; Fleury et al., 2009; Nexer et al.,
172 2015; Authemayou et al., 2018).

173

174 **2.2.2. Climate and hydrodynamics**

175

176 The climate affecting Sumba island is tropical, with humid winters and dry summers,
177 albeit relatively dry compared to other parts of Indonesia (Prasetia et al., 2013). The

178 mean annual precipitation in Sumba is $1077 \pm 406 \text{ mm a}^{-1}$ (average over the 1998-
179 2009 period of TRMM data; e.g., Kummerow et al., 2000).

180

181 The tides of Sumba Island have a range of $\sim 3.5 \text{ m}$ (Colas and Sutherland, 2001;
182 Alfonso-Sosa, 2016; Hibbert et al., 2016). Nevertheless, our study site (Cape Laundi)
183 is located on the northern, leeward side of the island which is only exposed to short
184 wavelength fetch swell ($< 10 \text{ s}$, i.e., windswell) (Butt et al., 2004).

185

186 **2.2.3. Previous studies on the Cape Laundi emerged coral reef** 187 **terraces sequence**

188

189 Cape Laundi was first mapped by Jouannic et al., (1988). It reaches $\sim 470 \text{ m}$ in
190 elevation and has a staircase shape with six main CRTs separated by continuous high
191 ($> 10 \text{ m}$) fossil sea cliffs (Pirazzoli et al., 1993). Each main CRT includes several
192 intermediate CRTs (Hantoro et al., 1989; Pirazzoli et al., 1993). Marine erosion was
193 detected by Pirazzoli et al. (1991; 1993) from the presence of marine notches in the
194 inner edges of main CRTs, and the observation of coral development surfaces marked
195 by traces of subsequent erosion observed along several canyons transversely cutting
196 the slope of the sequence.

197

198 Approximately fifty coral colonies have been dated (using U/Th and ESR dating
199 methods) on the surface of the five lowest main CRTs (T_1 to T_{IV1} in Pirazzoli et al.,
200 1993). These ages were correlated to eustatic peaks of the highstands associated,
201 respectively from the oldest to the youngest, to MIS 15 ($610 \pm 10 \text{ ka}$), MIS 11 ($390 \pm$
202 30 ka), MIS 9 ($325 \pm 18.5 \text{ ka}$), MIS 7 ($239.5 \pm 8.5 \text{ ka}$), MIS 5 ($122 \pm 6 \text{ ka}$) and MIS 1

203 (mid Holocene highstand, 6 ± 2 ka) (Pirazzoli et al., 1993; Bard et al., 1996). The oldest
204 dated CRT, named T_{IV1} in previous studies, yielded ESR ages of 584 ± 88 ka and 603
205 ± 90 ka and was corresponding to MIS 15 (Pirazzoli et al., 1991; 1993). At higher
206 elevations than T_{IV1} , the ages of the successive CRTs were extrapolated assuming a
207 constant uplift rate (i.e., 0.49 ± 0.01 mm a^{-1} ; Pirazzoli et al., 1993). The upper, undated
208 CRTs were thus correlated to sea level highstands up to ~ 1 Ma, i.e., MIS 29 (Jouannic
209 et al., 1988; Pirazzoli et al., 1991; 1993; Hantoro, 1992; Bard et al., 1996).

210

211 However, a number of temporal discrepancies emerged with the dating done by
212 Pirazzoli et al. (1991; 1993). Firstly, U-series ages of corals from the same CRT are
213 diachronic (e.g., ages of ~ 82 ka and ~ 138 ka from CRT I_1). Secondly, the same U-
214 series ages came from corals on at least three CRTs (e.g., MIS 5e ages on CRTs I_1 ,
215 I_2 , and II_2), and thirdly, U-series ages and ESR ages of corals from the same CRT do
216 not always match with one another. Thereafter, TIMS U-series dating of corals (Bard
217 et al., 1996) specified the diachronism (i.e., MIS 5a, 5c, and 5e ages on CRT I_1 ; MIS
218 5c, 5e and pre-MIS 5e ages on CRT I_2).

219

220 Bard et al. (1996) interpreted the age inconsistencies to reflect the decrease in uplift
221 rates during a significant period of the late Pleistocene. Very low uplift rates induce
222 negligible uplift of the lowest CRTs before the next transgression, resulting in one or
223 more reoccupation events in which new coral can grow on the pre-existing CRT (Fig.
224 1B). Combining $^{230}\text{Th}/\text{U}$ dating with numerical modeling, Bard et al. (1996) estimated
225 an uplift rate ranging from 0.2 to 0.5 mm a^{-1} and proposed also a polycyclic nature for
226 several CRTs (up to MIS 7). Low uplift rates (0.2 mm a^{-1}) allow coral colonies of a CRT
227 to be recovered by younger ones during a new transgression. But, to obtain the 0.2

228 mm a⁻¹ minimum uplift rate, the previous authors correlated the inner edge of the
229 lowermost main CRT (23 ± 2 m) to MIS 5e, taking into account only the oldest ²³⁰Th/U
230 ages. This hypothesis implies that during the MIS 5c and 5a highstands, coastal
231 erosion has been negligible to preserve the morphology of the MIS 5e CRT.

232

233 Pirazzoli et al. (1993) interpreted the age inconsistencies to reflect marine erosion.
234 Indeed, they suggested that eustatic sea level fluctuations with efficient marine
235 abrasion superimposed on a regular uplift trend of 0.5 mm a⁻¹ must have led sea level
236 to reach nearly the same position several times and the development of
237 bioconstructions differing in age as much as 100 ka on the same CRT (Fig. 1A). The
238 present altitude of dated CRTs allowed Pirazzoli et al. (1991; 1993) to propose an uplift
239 rate trend of 0.49 ± 0.01 mm a⁻¹.

240

241 **3. Methods**

242 **3.1. Mapping, bathymetry, and sampling**

243 **3.1.1. Onshore and offshore data**

244

245 We mapped the inner edges of the CRTs at Cape Laundi using a high resolution (2 m)
246 Digital Elevation Model (DEM) produced from stereoscopic satellite images (Pleides,
247 CNES) with MicMac freeware (e.g., Rupnik et al., 2016). We acquired topographic and
248 bathymetric profiles, using a real kinematic differential global positioning system (RTK
249 DGPS) onshore, and a Humminbird 700 series sonar offshore (Fig. 4). Onshore, our
250 profiles were carried out perpendicular to the main inner edges of the successive
251 CRTs, parallel to those proposed by Pirazzoli et al. (1993) and starting from the mean

252 sea level. Profile 1 crosses the whole CRTs sequence and Profile 2 focuses on the
253 lowest CRTs (Fig. 4).

254

255 The roughness of the successive CRTs increases with elevation and therefore age
256 because of continental denudation (e.g., epikarst). This roughness is the main source
257 of error in elevation, far beyond instrumental errors. Consequently, we assigned an
258 elevation uncertainty to all the field measurements as a function of the amplitude of the
259 observed natural landform roughness; ± 0.5 m for low standing landforms ($<250.5 \pm$
260 0.5 m in elevation); ± 1.5 m on the summit of Cape Laundi and the upper CRTs (>250.5
261 ± 0.5 m in elevation) (Fig. 5).

262

263 **3.1.2. Sampling strategy**

264

265 We extracted samples for $^{230}\text{Th}/\text{U}$ dating, by drilling two coral colonies in growth
266 positions (samples SUM17-10 and SUM17-13) located on the Holocene CRT (H), near
267 the modern shore (Figs. 3; 4). From the base (CRT H) to the summit of Cape Laundi
268 (CRT VI), we collected 34 samples from the non-vegetated surfaces of the reefal
269 limestones forming the CRTs for cosmogenic ^{36}Cl analysis (Figs. 3; 4). To investigate
270 the potential variability of denudation rates across a given CRT, we collected samples,
271 when possible, from 1) the inner edge, 2) the main surface and 3) the distal edge (Fig.
272 2).

273

274 Below 167.6 ± 0.5 m, intermediate CRTs are distinguishable in the field through fossil
275 sea cliffs (~ 3 m in height), separated by narrow (80-430 m wide) flat surfaces (Fig. 6).
276 For such CRTs, the distances between two successive sampling sites (i.e., inner edge,

277 main surface, and distal edge) typically range from 20 to 100 m. The CRTs higher than
278 167.6 ± 0.5 m are wider, typically from ~ 330 to $\sim 1\,300$ m wide, and our sampling
279 interval is ~ 500 m.

280

281 To constrain exposure age (i.e., the age at which the CRT emerged), in the case that
282 the concentration of ^{36}Cl decreases exponentially at depth (e.g., Braucher et al., 2011)
283 or to highlight several exposure events (i.e., reoccupation stages), in the case that ^{36}Cl
284 concentration peaks at a certain depth, we drilled the lowermost CRT (I_1) to get a
285 continuous ~ 2.5 m deep borehole (Fig. 4) (e.g., Braucher et al. 2009; 2011; Hein et al.
286 2009; Schaller et al. 2009). Because of the heterogeneity and porosity of the fossil
287 reefal limestone, our borehole broke into pieces, preventing us from precisely knowing
288 the depths of most of the individual samples. Only the depth of the deepest material
289 recovered from 2.5 ± 0.1 m below the surface of the CRT and the surface sample were
290 considered.

291

292 **3.2. Cosmogenic nuclides**

293

294 The ^{36}Cl cosmogenic concentration in rocks ($N(z,t)$, g^{-1} atom) as a function of depth (z ,
295 cm) and time (t , year) can be expressed as follows (Stone et al., 1994):

296

$$297 \quad \frac{\partial N(z,t)}{\partial t} = P(z) - \lambda N(z,t) - \varepsilon \frac{\partial N(z,t)}{\partial z} \quad (1)$$

298

299 z is the depth of a sample. Here, all but one sample (from the bottom of the core in the
300 lowermost CRT) have been collected from exposed bedrock surfaces ($z=0$), under a
301 surface that denudes at a rate ε (cm a^{-1}). $P(z)$ is the total production rate of ^{36}Cl (atom

302 $\text{g}^{-1} \text{rock a}^{-1}$), depending on 1) the cosmic radiation (itself affected by the following
303 parameters: latitude, elevation, topographic shielding, self-shielding (i.e., sample
304 thickness and depth)) passing through a rock of thickness z and 2) on the composition
305 of the rock (Gosse and Phillips, 2001). λ is the decay constant of ^{36}Cl ($\lambda = 2.303 \cdot 10^{-6}$
306 a^{-1}).

307

308 For all 34 samples, we selected the carbonate matrix containing as few coral fragments
309 as possible. Density measurements on these matrix samples averaged 2.5 g cm^{-3} .
310 Each sample was washed and the fraction 250-1000 μm extracted. About $\sim 100 \text{ g}$ of
311 each sample was then used for chemical analysis. We used a standard chlorine
312 extraction protocol, which includes several steps of leaching, designed to remove labile
313 Cl of meteoric origin from mineral surfaces (Stone et al., 1996; Merchel et al., 2008;
314 Schlagenhauf et al., 2010). More precisely, the procedure involved a cleaning process
315 by ultrapure water to remove any suspended particles, followed by a partial dissolution
316 process in 2M HNO_3 . Samples were then spiked with $\sim 270 \mu\text{g}$ of an enriched $^{35}\text{Cl}/^{37}\text{Cl}$
317 solution in order to determine the ^{35}Cl natural content. Then, the sample was fully
318 dissolved in 2M HNO_3 . Residues were filtered from the solution and weighted. 1 ml
319 solution aliquot was collected from the filtered solution for Ca determination. Then, Cl
320 was precipitated as AgCl using AgNO_3 . The precipitate was dissolved with ammonia
321 and sulfur was reduced by the addition of a saturated $\text{Ba}(\text{NO}_3)_2$ solution. Afterwards,
322 the solution was filtered and a second precipitation of AgCl was performed with HNO_3 .
323 The dried AgCl was finally measured with Accelerator Mass Spectrometry (AMS) at
324 CEREGE (Centre de Recherche et d'Enseignement de Géosciences de
325 l'Environnement) in Aix-en-Provence (France). ^{36}Cl production and denudation rates
326 were calculated following Schimmelpfennig et al. (2009) taking into account Sea-Level-

327 High-Latitude production rates for rapid neutron spallation reactions (42.2 ± 2 atoms
328 ^{36}Cl ($\text{g Ca}^{-1} \text{ a}^{-1}$); Braucher et al., 2011; Schimmelpfennig et al., 2011; 2014), negative
329 muons (Heisinger et al., 2002), the rate of epithermal neutron production from fast
330 neutrons (Phillips et al., 2001) and the production from radiogenic neutrons (Fabryka-
331 Martin, 1988; Phillips and Plummer, 1996) (more information related to ^{36}Cl production
332 is detailed in Appendix "A" of Schimmelpfennig et al., 2009). Topographic shielding
333 was calculated for each sample using the topographic shielding add-in for ArcGIS
334 software (Codilean, 2006). The scaling factors are calculated with CosmoCalc 1.7
335 macro (Vermeesch, 2007; Dunai, 2010). Major oxides (SiO_2 , TiO_2 , Al_2O_3 , Fe_2O_3 , MnO ,
336 MgO , CaO , Na_2O , K_2O , P_2O_5) and trace elements (Li, Be, Mo, Ba, Sm, Gd, Pb, Th, U,
337 B, Sc, Cr, Cr, Co, Ni, Rb, Sr) have been measured on the bulk samples (i.e., the size
338 fraction $< 250 \mu\text{m}$ collected after crushing), respectively by an ICP AES-Ultima 2-Jobin
339 Yvon and an HR-ICP-MS Element XR, at the LGO (Laboratoire Géosciences Océan,
340 IUEM) in Brest (France) to determine their impact on the ^{36}Cl production rate. The CO_2
341 concentration in samples is determined by weighing the samples, dissolving them in a
342 Gas bench and measuring the CO_2 produced (Pôle de Spectrométrie Océan,
343 Plateforme Isotopes Stables, IUEM, Brest, France).

344

345 The interaction of secondary cosmic rays with rocks exposed in the Earth's surface
346 produces cosmogenic isotopes (Gosse and Phillips, 2001). Four major interactions are
347 responsible for the production of cosmogenic isotopes, in order of importance:
348 spallation, muon capture, neutron activation, and alpha particle interaction (Bierman,
349 1994). Except for the production of ^{36}Cl by neutron capture, which peaks at a shallow
350 depth rather than at the surface, cosmogenic isotope production rates decrease
351 exponentially with depth until they stabilize (Stone et al., 1998). The abundance of

352 cosmogenic isotopes increases with exposure time until steady state, when production
353 and decay of the cosmogenic isotope are balanced (Schlagenhauf et al., 2010). More
354 precisely, when bedrock surfaces are exposed to cosmic ray particles and denuded at
355 a constant rate for long enough, the induced cosmogenic nuclide production
356 equilibrates the losses due to radioactive decay and mass removal linked to
357 denudation processes (Lal, 1991). The cosmogenic nuclide concentration reached at
358 this steady state is inversely proportional to the denudation rate of the surface (e.g.,
359 Granger and Riebe, 2014). The time it takes for the concentration of a cosmogenic
360 nuclide to reach steady state depends mainly on the denudation rate. When this steady
361 state is reached, it is possible to quantify the denudation rates without knowing the age
362 of the surface because for any age taken, and for a given ^{36}Cl concentration, the
363 denudation rate will not vary anymore (e.g., Lal et al., 1991; Dunai, 2010). Conversely,
364 for a surface sample that has not reached steady state and was taken on a surface
365 without age constraint, there is an infinite number of age-denudation pair hypotheses
366 that can explain the measured concentration. The denudation rate can be calculated
367 by assuming or independently constraining an exposure age (e.g., using absolute
368 chronological constraints such as $^{230}\text{Th}/\text{U}$ ages) and vice versa. Also, constraining both
369 exposure ages and denudation rates when steady state is not reached is possible by
370 fitting a theoretical depth profile, calculated from measured surface and depth
371 concentrations (Braucher et al. 2009; 2011; Hein et al. 2009; Schaller et al. 2009).

372

373 In this study, the denudation rates were calculated from ^{36}Cl concentrations assuming
374 a range of absolute ages for CRTs proposed by Pirazzoli et al. (1991; 1993). We show
375 that cosmogenic steady state has been reached for older CRTs than CRT II7
376 (corresponding to ~137 m altitude; Fig. 6) because denudation rates remain

377 unchanged regardless of the chosen age for the CRT. Thus, the age hypotheses are
378 useless to quantify denudation rates for these older CRTs (Section 4.4.). Samples on
379 CRTs surfaces yield continental denudation rates (Fig. 1C), while samples from CRT
380 H yield the quantification of marine erosion (Fig. 1A). Denudation rates are averaged
381 over the time period necessary to erode to a depth equivalent to the neutron
382 characteristic attenuation length (approximately 60 cm in a substrate with a density of
383 2.5 g cm^{-3}) (Von Blanckenburg, 2005).

384

385 **3.3. $^{230}\text{Th}/\text{U}$ dating**

386

387 On CRT H (Holocene), at the same sites as the lowest ^{36}Cl samples (SUM18-46 and
388 SUM18-47), we also sampled coral colonies of *Platygyra* (sample SUM17-10) and
389 *Favites* (sample SUM17-13 drilled in a fossil tidal pool) in growth position for $^{230}\text{Th}/\text{U}$
390 dating (Fig. 4). These $^{230}\text{Th}/\text{U}$ dating were done on CRT H in order to complete the
391 bibliographic data and to be as close as possible to the cosmogenic nuclide samples
392 to better discuss marine erosion processes. The two samples were mechanically
393 cleaned with a micro-drill and then crushed. Coral samples were rinsed in MilliQ water
394 and leached in 0.1 N bi-distilled HCL for 15-20 minutes in an ultrasonic bath. The
395 cleaned samples were then crushed into powder and analyzed using a XRD Brucker
396 D8 at the LCG (Laboratoire d'étude des "Cycles Géochimiques et Ressources",
397 IFREMER) in Brest (France) to quantify the relative quantities of calcite and aragonite.
398 We proceeded with $^{230}\text{Th}/\text{U}$ dating only with two samples, consisting purely of
399 aragonite (>99%).

400

401 Subsequently, the powders were dissolved in 7N HNO₃ and a mixed ²²⁹Th-²³³U-²³⁶U
402 spike was added to the solution and allowed to equilibrate. A detailed description of
403 the calibration of the spike is given by Gibert et al. (2016). After drying down the
404 solutions, the residues were treated with a mixture of concentrated HNO₃, HCl, and
405 H₂O₂ to remove potential organic components. Then, the solutions were dried again
406 and dissolved in 6N HCl. The fractions of U and Th were then separated from the
407 CaCO₃ matrix as described by Yang et al. (2015). For mass spectrometric analysis,
408 the U and Th fractions were dissolved in 2 ml of 0.8N HNO₃. U and Th isotope analysis
409 was performed by multi-collector inductively coupled plasma mass spectrometry at the
410 Institute for Geosciences of the Johannes Gutenberg-University, Mainz (Germany),
411 using a Thermo Fisher Scientific Neptune Plus MC-ICP-MS. A detailed description of
412 the analytical procedures is given by Obert et al. (2016).

413

414 **4. Results**

415 **4.1. Cape Laundi: offshore and onshore landforms**

416

417 Improved DEM resolution, new bathymetric data and field observations allowed us to
418 improve the mapping of Cape Laundi. The precise description of the coastal
419 morphology is essential to better understand the processes of its formation and
420 destruction. Offshore, two submerged ~200 m wide surfaces (named -l₁ and -l₂; Fig. 6),
421 were newly identified. Their morphology is consistent with paleo-lagoons: flat in their
422 central part (at -38 ± 1 and -53 ± 1 m for -l₁ and -l₂, respectively; Fig. 6) and convex at
423 their distal part associated with submerged barrier reefs (at -31 ± 1 and -44 ± 1 m for -
424 l₁ and -l₂, respectively; Fig. 6). We interpret these bathymetric features as submerged
425 CRTs.

426

427 Onshore, seven main CRTs were identified up to 469.8 ± 1.5 m with six major fossil
428 sea cliffs (Figs. 4; 5A; 6). Most of these main CRTs include intermediate CRTs. For
429 example, CRT II, with an inner edge raised at 136.8 ± 0.5 m, is composed of seven
430 intermediate CRTs (II₁, II₂, II₃, II₄, II₅, II₆, II₇) separated by low fossil sea cliffs (<10 m
431 each). The lowermost main CRT (CRT I) is 550 m wide, has an inner edge raised at
432 23.2 ± 0.5 m, and includes of two intermediate CRTs (I₁, I₂) separated at 6.4 ± 0.5 m
433 by a ~3 m high fossil sea cliff. On profile 2, CRT I is only 200 m wide, its surface is
434 irregular, and the two intermediate CRTs (I₁, I₂) are separated at 7.6 ± 0.5 m by a ~15
435 m high fossil sea cliff.

436

437 CRT I₁ consists of well-preserved smooth flat surfaces (Figs. 5C; 5D). In places, its
438 surface is covered by centimeter-scale remnants of a sandstone layer including coral
439 rubbles (Fig. 5E). The surface of CRT I₂ is irregular and exhibits some isolated smooth
440 multi-centimetric carbonate surfaces attesting for the relatively quick formation of rough
441 surfaces on the CRT. This superficial layer becomes rougher and thicker from CRT II₂,
442 where it reaches ~20 cm (Fig. 5B). At the highest CRTs, epikarstic roughness reaches
443 1 to 2 m (Figs. 5F; 5G). Moreover, the roughness varies across the CRTs, between
444 ~0.1 to ~2 m, i.e., the inner edges and the main surfaces of the CRTs are rather smooth
445 whereas their distal edges are rougher (Fig. 5G).

446

447 Alongshore, Holocene landforms are represented by a conglomerate, remnants of
448 limestone banks of fossil reef, and coral colonies in growth position, reaching
449 approximately 2 ± 0.5 m above mean sea level (Fig. 5C). Remnants of CRT H have a
450 restricted width (~5 m) and are delimited seaward by active sea cliffs (Fig. 5C). On the

451 flat surface of CRT H, some fossil corals appear very well-preserved and most
452 frequently located in circular depressions with their associated ramparts filled by a
453 white and fresh carbonated matrix (Fig. 5I). The diameter of such circular landforms is
454 generally ~1 m and we interpret them as fossil tidal pools (Fig. 5I) (Hoeksema, 2012).
455 Fossil coral colonies samples within this Holocene emergent reef have been previously
456 cross-dated from 2.03 ± 0.18 to 6.32 ± 0.14 (Jouannic et al., 1988; Pirazzoli et al.,
457 1991, 1993; Bard et al., 1996). The modern reef flat (called I_0 on Fig. 5B) is typical of
458 a fringing reef, as previously interpreted by Bard et al. (1996). There are living corals
459 on the reef crest (seaward), whereas landwards the reefal flat is covered by coral
460 rubbles (Fig. 5J) and associated with beaches and/or mangroves at some sites.

461

462 **4.2. $^{230}\text{Th}/\text{U}$ dating of the Holocene CRT**

463

464 The two fossil coral samples display ^{238}U concentrations between 2.4 and 3 ppm (Table
465 1). Low ^{232}Th contents together with high ($^{230}\text{Th}/^{232}\text{Th}$) activity ratios argue for a lack of
466 significant detrital contamination. Both samples display initial $\delta^{234}\text{U}$ values that agree
467 within errors with a mean modern ocean water value of $\delta^{234}\text{U} = 146.8 \pm 0.1\text{‰}$
468 (Andersen et al., 2010), indicating closed system evolution and no evidence for
469 diagenetic alteration. These coral colonies samples yielded $^{230}\text{Th}/\text{U}$ ages of 5.45 ± 0.02
470 ka (sample SUM17-10) and 2.13 ± 0.01 ka (sample SUM17-13) (Table 1).

471

472 **4.3. Distribution of ^{36}Cl concentration at the scale of the emerged coral** 473 **reef terraces sequence**

474

475 The ^{36}Cl concentrations obtained from the samples along profiles 1 and 2 range from
476 3.68 ± 0.08 to $20.00 \pm 0.37 \cdot 10^5$ atoms g^{-1} rock and average at $7.74 \pm 3.67 \cdot 10^5$ atoms
477 g^{-1} rock ($n = 28$; Table 2). Given the overall uniform lithology and precipitation rate, the
478 variability across the profile is higher than expected if all measured ^{36}Cl concentrations
479 have been controlled by steady erosion. The six measured ^{36}Cl concentrations of
480 samples from CRT I have low variability (with an average at $5.54 \pm 0.67 \cdot 10^5$ atoms g^{-1}
481 rock) compared to the ^{36}Cl concentration of all other/older samples (with an average
482 at $8.25 \pm 3.90 \cdot 10^5$ atoms g^{-1} rock). The ^{36}Cl concentration measured at the base
483 (sample SUM18-47: $0.30 \pm 0.05 \cdot 10^5$ atoms g^{-1} rock) and on the top of the modern sea
484 cliff (sample SUM18-46: $0.38 \pm 0.08 \cdot 10^5$ atoms g^{-1} rock) are an order of magnitude
485 lower than those measured on Pleistocene CRTs (I-VII) (Table 2). At the borehole site
486 (Fig. 4), the ^{36}Cl concentrations measured at the surface (C_{surface}) and at a depth of
487 2.5 ± 0.1 m ($C_{\text{2.5m}}$) are 6.23 ± 0.28 and $2.46 \pm 0.12 \cdot 10^5$ atoms g^{-1} rock, respectively
488 (Table 2).

489

490 **4.4. Denudation rates**

491

492 The time scales over which denudation rates are integrated (Von Blanckenburg, 2005)
493 range from 16.2 ± 0.3 (highest rate) to 237.3 ± 27.0 ka (lowest rate) with an average
494 of 61.7 ± 49.6 ka ($n = 66$). Denudation rates for the various CRTs of the sequence
495 range from 2.5 ± 0.1 to 37.1 ± 0.9 mm ka^{-1} (average at 14.7 ± 8.3 mm ka^{-1} , $n = 66$)
496 (Table 3; Fig. 6). Despite the different age hypotheses for CRT I, the denudation rates
497 calculated are more uniform than those determined for the upper CRTs (Table 3; Fig.
498 6). Denudation rates from the CRTs II₂, II₃, and II₄ are rather similar, irrespective of
499 different age hypotheses (Table 3; Fig. 6). The results suggest that cosmogenic steady

500 state has been reached for older CRTs than II₇; i.e., whatever the assigned age to the
501 CRT, the calculated denudation rates for these CRTs do not vary much (Table 3; Fig.
502 6).

503

504 The average denudation rates affecting the inner edges, main surfaces and distal
505 edges of the CRTs are 11.1 ± 7.0 (n = 16), 14.3 ± 6.8 (n = 38), and 20.8 ± 8.6 mm ka⁻¹
506 (n = 12) respectively. Denudation rates for CRTs main surfaces are widely dispersed
507 and range from 2.5 ± 0.3 (sample SUM18-37) to 29.4 ± 1.4 mm ka⁻¹ (sample SUM16-
508 8). Apart from the denudation rate calculated for sample SUM18-15 (Table 3),
509 denudation rates affecting the inner edges of CRTs I₁, II₁, II₄, II₆, V, VI are similar to
510 those of the fossil reef flats. Denudation rates for the distal edge of the CRTs are higher
511 than rates from other parts of the landform. Since the number of denudation rate values
512 is low, a non-parametric statistical test was performed (Kruskal-Wallis test) to
513 determine whether denudation rates vary significantly by morphological location of the
514 samples analyzed. The average rank of the calculated denudation rates is not
515 statistically significantly different according to the morphological location of the
516 samples ($P_{\text{value}} = 0.26$). Thus, the morphology of the CRTs does not fully explain the
517 heterogeneity of the calculated denudation rates.

518

519 Sample SUM18-46 was collected from the same surface (CRT H) of the samples used
520 for ²³⁰Th/U dating (SUM17-10 and SUM17-13) (Figs. 4; 5C). Considering ²³⁰Th/U ages
521 as the exposure time of the surface, we calculated denudation rates of 279.0 ± 0.4 mm
522 ka⁻¹ and 581.0 ± 0.4 mm ka⁻¹ (Table 3). These denudation rates (average of 430 ± 214
523 mm ka⁻¹; Table 3) near the sea level are much higher, by one to two orders of
524 magnitude, than the denudation rates calculated for the other CRTs (I-VI).

525

526 **5. Discussion**

527

528 Significant denudation rates obtained at the sea level and on the CRTs sequence point
529 to marine erosion and continental denudation as the cause of the age diachronism on
530 a single CRT (Figs. 1A; 1B). This hypothesis also requires reef reoccupation over
531 several highstands (R2 over R1 on figure 1). Our results provide the opportunity to
532 discuss the dynamics of these processes at Cape Laundi. We first highlight the role of
533 reef reoccupation processes and marine erosion in shaping CRTs. Then, we discuss
534 continental denudation by comparing our data with denudation rates published for the
535 Barbados and Puerto Rico CRTs (Lal et al., 2005), as well as for other carbonate
536 landscapes (e.g., Spencer, 1985; Vasconcelos and Stone, 2000), and focusing on the
537 variability of denudation rates.

538

539 **5.1. The genesis of the lowermost main CRT (I)**

540 **5.1.1. Reefal limestone units overlapping**

541

542 Whatever the hypothesis to explain diachronous ages on the same CRT surface, the
543 CRT internal architecture must be associated with a phenomenon of reef reoccupation
544 over several highstands in order to have recent thin reef units stacked on older units
545 (R2 over R1 in figure 1). In the borehole site of CRT 1, theoretically, if both measured
546 samples belong to the same reefal limestone unit, the ^{36}Cl concentration profile in
547 depth (constrained by an erosion rate and age) should decrease exponentially and join
548 the two measured ^{36}Cl concentration points. To construct this profile, we (1) made
549 different age hypotheses for CRT I₁, (2) used the ^{36}Cl concentration measured at the

550 surface ($C_{m_{\text{surface}}}$) to start the profile, (3) set the denudation rate automatically by
551 combining the measured ^{36}Cl concentration at the surface ($C_{m_{\text{surface}}}$) with the chosen
552 hypothetical age, and (4) set a minimum and a maximum of reef porosity from 0% (i.e.,
553 density 2.5 g cm^{-3}) to 50 % (i.e., a density of 1.25 g cm^{-3}) (e.g., Smith, 1983). We test
554 the ages proposed by Pirazzoli et al. (1991; 1993): MIS 5e, c and a, as well as an
555 extremely old age, i.e., 1.5 Ma, to test a steady state hypothesis (Schimmelpfennig et
556 al., 2009).

557

558 In any case, it is not possible to join the two ^{36}Cl concentrations measured by the
559 theoretical ^{36}Cl concentration profiles (Fig. 7). Regardless of the scenario, the 2.5 ± 0.1
560 m deep sample exhibits a ^{36}Cl concentration higher than its theoretical estimate (Fig.
561 7). The only exception is observed with a 50% porosity and the age of the drilled unit
562 estimated at 1.5 Ma. However, this age is too old compared to the dating done by
563 previous authors on the studied CRT (Pirazzoli et al., 1991; 1993; Bard et al., 1996).
564 The only way to explain the high ^{36}Cl concentration of the sample at 2.5 ± 0.1 m is that
565 this reefal limestone unit has been exposed to cosmic radiation before an overlapping
566 unit was emplaced, i.e., in a later stage of reoccupation. It follows that the borehole
567 goes through two reefal limestone units, the upper one being thinner than 2.5 m.

568

569 We thus hypothesize that this difference in the ^{36}Cl concentrations measured has been
570 acquired on the temporarily emerged surface of the CRT between two successive
571 highstands. We then calculate exposure times before overlapping with Δc (i.e.,
572 difference between the measured and theoretical ^{36}Cl concentration at a depth of 2.5
573 m; Table 4) according to possible ages of MIS 5a, MIS 5c and MIS 5e for the surface
574 unit ($Ed_{\Delta c}$ in Table 4; Pirazzoli et al., 1991; 1993; Bard et al., 1996). These values

575 correspond to minimum exposure time because after overlapping, the ^{36}Cl
576 concentration decreases with isotopic decay. Considering the ages of MIS 5e, 5c and
577 5a, which are 122 ± 6 ka, 100 ± 5 ka, and 82 ± 3 ka, respectively (Cutler et al., 2003),
578 the time intervals between isotopic stages 5e-5c, 5c-5a and 5e-5a are 22 ± 11 ka, 18
579 ± 8 ka, and 40 ± 9 ka, respectively. For the zero-porosity hypothesis, the calculated
580 exposure times before overlapping (13.8 ± 1.3 ka, 12.5 ± 1.2 ka, and 11.0 ± 1.2 ka) are
581 equivalent to the time intervals between two successive substages of MIS 5 (Table 4).
582 Consequently, our data argue that the borehole intersected two units that could be
583 associated to the two of the three relative highstands of the last interglacial: MIS 5a
584 and 5c, or MIS 5c and 5e (Table 4; Fig. 7).

585

586 We conclude that the ^{36}Cl borehole method confirms previous observations deduced
587 from $^{230}\text{Th}/\text{U}$ ages (Pirazzoli et al., 1991; 1993; Bard et al., 1996), and that CRT I₁ is
588 composite and was built during at least two successive highstands of the last
589 interglacial.

590

591 **5.1.2. Evidence for marine erosion and constructive reoccupation**

592

593 Combining cosmogenic nuclide analyses and $^{230}\text{Th}/\text{U}$ dating on reef samples collected
594 near sea level allows to discuss the hypothesis of Pirazzoli et al., (1993) that reef
595 reoccupation is associated with marine erosion (Fig. 1A). Our two samples from CRT
596 H, one at the base (SUM18-47, $0.30 \pm 0.03 \cdot 10^5$ atoms g^{-1} rock) and the other at the
597 top of the modern sea cliff (SUM18-46, $0.38 \pm 0.04 \cdot 10^5$ atoms g^{-1} rock), give similar
598 low ^{36}Cl concentrations (Table 2). If sample SUM18-47 had been recently exposed by
599 sea cliff retreat, its ^{36}Cl concentration would be much lower (e.g., Regard et al., 2012).

600 Therefore, the two samples at the top and the base of the modern sea cliff likely
601 experienced the same erosive history over the time interval resolved by the ^{36}Cl
602 method (~ 1.5 ka). In view of their location close to sea level and the high denudation
603 rates calculated from the top of the modern sea cliff (average of 430 ± 214 mm ka^{-1}),
604 the erosion process is most likely marine. The efficiency of marine erosion has already
605 been demonstrated by numerous studies, in particular using cosmonuclides (Gibb,
606 1978; Spencer, 1985; Stephenson and Kirk, 1998; Brown et al., 2003; Raimbault et al.,
607 2018). In Grand Cayman Island, the average marine erosion rate affecting reef
608 shielded coasts is 450 mm ka^{-1} (Spencer, 1985), which is in agreement with our
609 denudation rate values. However, denudation rates affecting the active sea cliff at
610 Cape Laundi were calculated on small length (sample of few centimeters) and time
611 (age hypothesis of few thousand years) scales. It may reflect the stochastic nature of
612 erosion, i.e., the detachment of a small block that can generate a large difference on
613 the calculated denudation rates. Such efficient erosion at sea level during a relatively
614 short period of time can be caused by extreme events, such as storms, cyclones, or
615 tsunamis (Anderson et al., 1999). Consequently, a comparison with denudation rates
616 averaged over much larger temporal and spatial scales may be misleading.

617

618 Whatever the uplift rate or the value of the glacial isostatic adjustment, the location of
619 the samples dated at 5.45 ± 0.02 ka and 2.13 ± 0.01 ka at the same altitude and a few
620 metres apart can only be explained by erosion and reoccupation. In addition, we have
621 observed fossil tidal pools on the CRT H surface (Fig. 5I), where the coral dated as
622 2.13 ± 0.01 ka was sampled, which allows us to specify the reoccupation mode.
623 Therefore, we interpret the coral dated at 2.13 ± 0.01 ka (SUM17-13) as a coral-colony
624 that settled on the top surface of the active sea cliff in fossil tidal pools fed by seawater

625 during high tides or storms, as observed elsewhere (e.g., Hoeksema, 2012). As such,
626 we conclude that the constructive reoccupation affected the CRT H during the Mid-
627 Holocene with a partial immersion of the reef platform.

628

629 **5.1.3. Argument of the abandonment of the main CRT (I) in a single** 630 **eustatic event.**

631

632 Cosmogenic nuclide data also inform us about the processes of CRT abandonment
633 during regression. CRT I is not old enough to have reached cosmogenic steady state.
634 However, ^{36}Cl concentrations measured on the main CRT I (I_1 , I_2) are uniform (Table
635 2, Fig. 6), suggesting a similar exposure time to radiation for the whole surface of CRT
636 I. Thus, the abandonment of CRT I surface most probably corresponds to a discrete,
637 single event, during regression after the last interglacial highstand.

638

639 **5.2. Continental denudation of CRTs**

640 **5.2.1. Comparison with global trends of carbonate denudation** 641 **rates**

642

643 In previous studies, continental denudation of reef carbonate landforms has been
644 quantified by taking direct *in situ* measurements, for example, ^{36}Cl concentrations (Lal
645 et al., 2005) as well as micro-erosion (e.g., Trudgill, 1976; 1979). Each method is
646 representative of a given period of time on which the calculated denudation rates are
647 integrated. For the ^{36}Cl method, this period is between 10^3 to 10^5 years. In contrast,
648 the micro-erosion method covers periods of only one to two years (e.g., Trudgill, 1976;
649 Spencer, 1985).

650

651 Denudation rates at Cap Laundi (average of $14.7 \pm 8.3 \text{ mm ka}^{-1}$), where precipitation
652 rates are $\sim 1000 \text{ mm a}^{-1}$, are lower than those of tropical sites with higher rainfall ($>$
653 2000 mm a^{-1}), such as in Papua New Guinea (denudation rate of $\sim 150 \text{ mm ka}^{-1}$,
654 Vasconcelos and Stone, 2000), higher than those obtained in arid to hyper-arid zones
655 (denudation rate of from 1 to 3 mm ka^{-1} , Ryb et al., 2014) and similar to those derived
656 with the same method (^{36}Cl concentration) on the same features (upper Pleistocene
657 CRTs) at locations with the same mean annual precipitation rates (1200 - 1500 mm a^{-1}
658 in Rendezvous Hill, Barbados and $\sim 915 \text{ mm a}^{-1}$ in Isla Mona, Puerto Rico). Denudation
659 rates range from 7 to 118 mm ka^{-1} on the Rendezvous Hill and from 26 to 61 mm ka^{-1}
660 at Isla Mona (Lal et al., 2005). Trudgill (1976; 1979) obtained similar denudation rates
661 (9 - 62 mm ka^{-1}) in Aldabra atoll (Seychelles archipelago), that receives comparable
662 rainfalls (Shekeine et al., 2015). Thus, denudation rates calculated at Cape Laundi are
663 consistent with the global correlation between rainfall and denudation rates determined
664 by the *in situ* ^{36}Cl method on carbonate flat surfaces (Ryb et al., 2014; Levenson et al.,
665 2017). These continental denudation rates imply a surface stripping rate of 0.7 to 2.3
666 m per glacial/interglacial cycle. If the younger reef unit are thin as suggested by the
667 drilling results, this stripping is sufficient to reveal older reef units at the surface (Fig.
668 1C).

669

670 **5.2.2. Heterogeneous variations of denudation rates across the**

671 **sequence as well as individual CRT**

672

673 Denudation rates (i.e., ^{36}Cl concentrations) vary across the sequence, as well as within
674 each CRT. In the following, we propose that this is mainly due to the sampling bias

675 related to the roughness of the carbonate surfaces and the staircase morphology of
676 the sequence.

677

678 **5.2.2.1. Roughness versus ^{36}Cl concentrations**

679

680 Over time, aerial dissolution forms larger and larger dissolution pits, amplifying the
681 roughness of the CRT (Figs. 5A; 5B; 5F; 5G). Thus, at Cape Laundi, the older the CRT,
682 the rougher it is (Figs. 5A; 5B; 5F; 5G). The roughness of all CRTs is in the order of
683 decimeters (Fig. 5B). We also observed a coastal karren-type epikarstification (e.g.,
684 Lundberg, 2019). This process induces a detachment of 10 to 50 cm thick blocks from
685 the CRT surface (Figs. 5B; 8A; 8B). The types of corals, sediments, and stage of
686 cementation produce distinctive layers of limestone rocks in fossilized reefs (James
687 and Macintyre, 1985). The layering of the paleo-reef could therefore play an important
688 role in the development of these karstic forms (Figs. 8A; 8B).

689

690 Block detachment could produce a change of ^{36}Cl concentrations over the CRTs
691 surfaces with low values on recently dismantled zones. The following goal is to get an
692 independent estimate of the typical block size removed by these karstification
693 processes using our ^{36}Cl data. We selected two pairs of surface samples from the flat
694 part of the same CRT that yield different ^{36}Cl concentrations (SUM18-21/SUM16-4 and
695 SUM18-20/SUM16-10) and we hypothesized that the difference in ^{36}Cl concentration
696 values for each pair is related to the dismantling of the surface blocks. The pairs are
697 located on CRTs I₂ and II₄, respectively (Fig. 8C). We calculate the theoretical depth
698 profile of ^{36}Cl concentrations from the CRTs age inferred by Pirazzoli et al. (1991; 1993)
699 combined with the measured ^{36}Cl concentration for the most concentrated surface

700 sample (Fig. 8C). To quantify the stripped thickness required to achieve the lowest ^{36}Cl
701 concentration of each pair, we projected this concentration onto the calculated
702 theoretical depth profile of ^{36}Cl concentrations (Fig. 8C). We obtained stripped
703 thicknesses of ~30 cm and ~82 cm for CRTs I₂ and II₄, respectively (Fig. 8C). These
704 results are consistent with the natural roughness observed and the height generated
705 by the detachment of a block (Figs. 5B; 8A). Thus, the difference in ^{36}Cl concentration
706 between each pair of samples can be attributed to the removal of a single block.
707 Variations in ^{36}Cl concentration on the same CRT can be explained by the spatial
708 variations of the degradation of the initial CRT surface. The greater the thickness of
709 the removed blocks, the greater the variations in ^{36}Cl concentration at the surface
710 related to its dismantling will be (Figs. 8B; 8C). Such spatial variations in denudation
711 rates imply that it is impossible to accurately date, with the analysis cosmogenic ^{36}Cl
712 concentrations, a CRT that has not yet reached the steady state (such as CRT I)
713 because it requires having a uniform value of this parameter all along the CRT.
714 Besides, these results suggest that on a given polycyclic CRT, the continental
715 denudation can partially strip the thin superficial layer of a young fossil coral reef and
716 exhume older corals in several places.

717

718 **5.2.2.2. CRT morphology versus ^{36}Cl concentrations**

719

720 When samples are divided according to their distribution on the CRT (i.e., inner edge,
721 terrace main surface, and distal edge) (Table 3), denudation rates reveal different
722 averages, with the highest values for the distal edges (Fig. 9). Although the non-
723 parametric statistical test (Kruskal-Wallis test) reveals that there is no significant
724 difference in denudation rates as a function of the morphological location of the sample

725 analyzed ($P_{\text{value}} = 0.26$), we consider that the distal edges are the most sensitive to
726 continental denudation because of their position at the top of the slope (Figs. 2; 6). In
727 this case, distal edges could be faster dissolved by diffusion between the fossil sea cliff
728 and fossil reef flat, and regressive erosion associated with runoff on the cliff. The flat
729 geometry of the CRT main surfaces prevents diffusion and runoff that could increase
730 the denudation rate. Furthermore, there may be a change in porosity between the main
731 surface and the distal edge of CRTs that may cause the dissolution rate to vary
732 spatially. The main surfaces of CRTs, considered a paleo lagoon (Cabioch, 2011), can
733 be then partly formed by the compaction and deposition of marine cements (Figs. 5C;
734 5D; 5E; Hopley, 2011), which reduces the porosity of the framework. The distal edges
735 of the CRTs, considered as the paleo reef crests (e.g., Pirazzoli et al., 1991; Rovere et
736 al., 2016), therefore appear to have a higher porosity than the main surfaces. The
737 greater the porosity, the more it allows the infiltration of meteoric water, accelerating
738 chemical dissolution and therefore potentially the denudation rate. Which in turn
739 explains the high roughness of the distal edges compared to other parts of the CRTs
740 (Fig. 5G).

741

742 **5.2.2.3. Water, sands cover and soil formation on CRT**

743 **versus ^{36}Cl concentration**

744

745 CRTs may be flooded during the subsequent interglacial substages if uplift rates are
746 low or if marine erosion lowers the CRT (Fig. 1). This process could play a role in
747 shielding and affect the production of ^{36}Cl on CRTs older than Holocene. However, the
748 integration time of the denudation rates calculated here (i.e., 61.7 ± 49.6 ka in average)
749 is too short to have recorded several highstands.

750

751 Besides, CRTs may also be covered by sand and debris during and after periods of
752 intense marine erosion. Indeed, we observed that CRT I₁ surface is covered by
753 centimeter-scale remnants of a sandstone layer including coral rubbles (Fig. 5E). The
754 process that forms this layer may be related to marine diagenetic cementation (Rasser
755 and Riegl, 2002). Storms are the natural events that generally explain the formation
756 and deposition of these layers (e.g., Scoffin, 1993; Bourrouilh-Le Jan, 1998; Blanchon
757 et al. 1997; Rasser and Riegl, 2002). Yet, they are also common features in sites
758 characterised by gently sloping, pre-existing surfaces (i.e., composite CRTs in our
759 study site) and medium wave energy (Cabioch et al., 1995). These sand patches are
760 widely scattered on the lower CRTs and are absent on the upper CRTs due to
761 continental denudation. They must have been removed during the CRT emergence by
762 marine erosion (only a few pieces remain; Figs. 5C; 5E) and by continental denudation
763 after the reef emersion. With a continental denudation rate of $14.7 \pm 8.3 \text{ mm ka}^{-1}$ on
764 average, it takes only ~7000 years to strip off a few tens of centimeters. Besides, this
765 thickness is too small to significantly affect the denudation rates and to be distinguished
766 from the stripping effect.

767

768 Our field observations have shown that soil is almost non-existent on the lowest CRTs
769 (Figs. 5D; 5E) and the soil on CRTs above CRT III is very thin (a few millimeters to
770 centimeters) and only allows the formation of vegetation of steppe moor (Figs. 5A; 5B;
771 5D; 5F; 5G). The relatively dry climate of the Cape Laundi region (e.g., Prasetia et al.,
772 2013) may be the cause of the lack of thick soil, which can affect the production of ³⁶Cl.
773 But despite this arid climate, the contribution of volcanic ash from the Sunda-Banda
774 arc or of Australian dust could favour the development of soil. This has already been

775 observed in Barbados, where the parent materials of the soils on uplifted CRTs are
776 Sahara dust and volcanic ash from the Lesser Antilles Island arc (Muhs, 2001). Similar
777 examples have been reported in Taiwan (Liew and Hsieh, 2000) as well as in Liuchiu
778 Island (Cheng et al., 2011). It remains an open question whether deforestation (e.g.,
779 Orr et al, 2012) and agricultural burning (e.g., Russell-Smith et al., 2007) could have
780 removed the soil formed over time, despite the low runoff induced by the horizontality
781 of the surfaces of the CRT. We have not observed any soil trapped and preserved in
782 the dissolution features (i.e., coastal karren; Lundberg, 2019) or superficial cracks of
783 the CRTs to testify to its previous existence. Over time, soil forms from the *in situ*
784 weathering of the initial surface of the CRT and thickens. An older CRT should
785 therefore have a thicker soil, a more weathered surface and be more protected from
786 cosmic rays (shielding action) than a more recent CRT. Thus, we should have
787 observed a decrease in the ^{36}Cl concentration with the age of the CRT with former
788 thick soil now gone. We have not observed such a trend in our data. Therefore, we
789 have no evidence of the influence of soils on the ^{36}Cl production in the CRTs at Cape
790 Laundi.

791

792 **6. Conclusions**

793

794 At Cape Laundi, previous studies (Pirazzoli et al., 1991; 1993; Bard et al., 1996) have
795 identified age discrepancies on CRTs. We disentangled the roles of continental
796 denudation, coastal erosion, and marine reoccupation in the promiscuity of diachron
797 coral colonies on the same CRT surface. The ^{36}Cl concentrations of 34 surface
798 limestone samples taken from different morphological zones of this CRTs sequence
799 allowed us to calculate continental denudation rates, ranging from 2.5 ± 0.3 to $37.1 \pm$

800 0.1 mm ka⁻¹ (14.7 ± 8.3 mm ka⁻¹ on average). The combined analysis of ²³⁰Th/U ages
801 and cosmogenic ³⁶Cl concentrations of surface and depth samples in both the distal
802 and proximal part of the lowermost CRT suggest that this CRT is composite and
803 records a polycyclic history with alternating construction and erosion phases during the
804 eustatic sea level variations of the last interglacial highstands (MIS 5e, 5c, and 5a) and
805 during the Mid-Holocene. Our results also highlight 1) significant spatial variability in
806 denudation rates, probably related to roughness and morphological zoning of CRTs,
807 which could bring coral colonies of different ages to the surface depending on the
808 efficiency of continental denudation, and 2) higher denudation rates affecting the distal
809 edges of CRTs than in other parts of the landform. Eventually, we stress that such
810 erosion processes, suggested since a long time but rarely discussed in the literature,
811 should be systematically taken into account when establishing the morphostratigraphy
812 of emerged coral reef terrace sequences.

813

814 **Acknowledgements**

815

816 This work was supported by public funds received in the framework of GEOSUD, a
817 project (ANR-10-EQPX-20 and ANR-10-LABX-19-01, Labex Mer, CLIMORESO, C.
818 Authemayou) of the program "Investissements d'Avenir" managed by the French
819 National Research Agency, the INSU Tellus Syter program (SECOMAS, C.
820 Authemayou) and the CNES TOSCA program (CETTROPICO, C. Authemayou). We
821 thank the German Aerospace Center for providing us the TanDEM-X data for our study
822 zone. We thank the State Ministry of Research and Technology of Indonesia "RISTEK"
823 that allowed us to conduct the field trip to Sumba (research permit
824 680/FRP/E5/Dit.KI/IV/2017). We also thank the National Geographic Explorer grant

825 (no CP 087R 17) to support the Indonesian researchers (Sri Yudawati Cahyarini, Vera
826 Christanti Agusta, and Danny Hilman Natawidjaja). Denis Scholz is thankful to the DFG
827 for funding (SCHO 1274/11-1 and INST 247/889-1 FUGG). We thank Gilles Brocard
828 for his help with karstic terminology. Finally, we thank 3 anonymous reviewers for
829 fruitful discussions on former versions of this manuscript.

830

831 **References cited**

832

833 1. Abdullah, C. I., Rampnoux, J. P., Bellon, H., Maury, R. C., & Soeria-Atmadja, R.
834 (2000). The evolution of Sumba Island (Indonesia) revisited in the light of new
835 data on the geochronology and geochemistry of the magmatic rocks. *Journal of*
836 *Asian Earth Sciences*, 18(5), 533-546.

837

838 2. Alfonso-Sosa, E. (2016). Tidal mixing in the Sumba Strait and internal wave
839 activity detected during strong semidiurnal forcing.

840

841 3. Andersen, M. B., Stirling, C. H., Zimmermann, B., & Halliday, A. N. (2010).
842 Precise determination of the open ocean $^{234}\text{U}/^{238}\text{U}$ composition.
843 *Geochemistry, Geophysics, Geosystems*, 11(12).

844

845 4. Anderson, R. S., Densmore, A. L., & Ellis, M. A. (1999). The generation and
846 degradation of marine terraces. *Basin Research*, 11(1), 7-20.

847

848 5. Authemayou, C., Brocard, G., Delcaillau, B., Molliex, S. p., Pedoja, K., Husson,
849 L., et al. (2018). Unraveling the roles of asymmetric uplift, normal faulting and

- 850 groundwater flow to drainage rearrangement in an emerging karstic landscape.
851 Earth Surface Processes and Landforms, 43(9), 1885-1898.
852
- 853 **6.** Bard, E., Jouannic, C., Hamelin, B., Pirazzoli, P., Arnold, M., Faure, G., et al.
854 (1996). Pleistocene sea levels and tectonic uplift based on dating of corals from
855 Sumba Island, Indonesia. Geophysical Research Letters, 23(12), 1473-1476.
856
- 857 **7.** Bierman, P. R. (1994). Using in situ produced cosmogenic isotopes to estimate
858 rates of landscape evolution: A review from the geomorphic perspective.
859 Journal of Geophysical Research: Solid Earth, 99(B7), 13885-13896.
860
- 861 **8.** Blanchon, P., Jones, B., & Kalbfleisch, W. (1997). Anatomy of a fringing reef
862 around Grand Cayman; storm rubble, not coral framework. Journal of
863 Sedimentary Research, 67(1), 1-16.
864
- 865 **9.** Bourrouilh-Le Jan, F. G. (1998). The role of high-energy events (hurricanes
866 and/or tsunamis) in the sedimentation, diagenesis and karst initiation of tropical
867 shallow water carbonate platforms and atolls. Sedimentary Geology, 118(1-4),
868 3-36.
869
- 870 **10.** Braucher, R., Del Castillo, P., Siame, L., Hidy, A. J., & Bourles, D. L. (2009).
871 Determination of both exposure time and denudation rate from an in situ-
872 produced ¹⁰Be depth profile: a mathematical proof of uniqueness. Model
873 sensitivity and applications to natural cases. Quaternary Geochronology, 4(1),
874 56-67.

875

876 **11.**Braucher, R., Merchel, S., Borgomano, J., & Bourlès, D. L. (2011). Production
877 of cosmogenic radionuclides at great depth: a multi element approach. Earth
878 and Planetary Science Letters, 309(1-2), 1-9.

879

880 **12.**Brown, J., Jorgenson, M. T., Smith, O. P., & Lee, W. (2003). Long-term rates of
881 coastal erosion and carbon input, Elson Lagoon, Barrow, Alaska. Paper
882 presented at the Eighth International Conference on Permafrost.

883

884 **13.**Butt, T., Russell, P., & Grigg, R. (2004). Surf science: An introduction to waves
885 for surfing: University of Hawaii Press Honolulu.

886

887 **14.**Cabioch, G., Montaggioni, L. F., & Faure, G. (1995). Holocene initiation and
888 development of New Caledonian fringing reefs, SW Pacific. Coral Reefs, 14(3),
889 131-140.

890

891 **15.**Cabioch, G. (2011). Emerged reefs. Encyclopedia of Modern Coral Reefs:
892 Structure, Form and Process, 373-380.

893

894 **16.**Chappell, J. (1974). Geology of coral terraces, Huon Peninsula, New Guinea: a
895 study of Quaternary tectonic movements and sea-level changes. Geological
896 Society of America Bulletin, 85(4), 553-570.

897

898 **17.**Cheng, C.-H., Jien, S.-H., Tsai, H., & Hseu, Z.-Y. (2011). Geomorphological and
899 paleoclimatic implications of soil development from siliceous materials on the

900 coral-reef terraces of Liuchiu Island in southern Taiwan. Soil science and plant
901 nutrition, 57(1), 114-127.

902

903 **18.**Codilean, A. T. (2006). Calculation of the cosmogenic nuclide production
904 topographic shielding scaling factor for large areas using DEMs. Earth Surface
905 Processes and Landforms, 31(6), 785-794.

906

907 **19.**Colas, A., & Sutherland, B. (2001). The world stormrider guide: Low Pressure.

908

909 **20.**Crosby, W. O. (1883). Elevated coral reefs of cuba. Journal of Natural History,
910 12(70), 283-284.

911

912 **21.**Cutler, K. B., Edwards, R. L., Taylor, F. W., Cheng, H., Adkins, J., Gallup, C. D.,
913 et al. (2003). Rapid sea-level fall and deep-ocean temperature change since the
914 last interglacial period. Earth and Planetary Science Letters, 206(3-4), 253-271.

915

916 **22.**Daly, R. A. (1915). The glacial-control theory of coral reefs.

917

918 **23.**Darwin, C. (1842). The Structure and Distribution of Coral Reefs: Being the First
919 Part of the Geology of the Voyage of the Beagle... During the Years 1832-1836:
920 Smith, Elder.

921

922 **24.**Dunai, T. J. (2010). Cosmogenic Nuclides: Principles, concepts and
923 applications in the Earth surface sciences: Cambridge University Press.

924

- 925 **25.** Fabryka-Martin, J. T. (1988). Production of radionuclides in the earth and their
926 hydrogeologic significance, with emphasis on chlorine-36 and iodine-129.
927
- 928 **26.** Fleury, J.-M., Pubellier, M., & de Urreiztieta, M. (2009). Structural expression of
929 forearc crust uplift due to subducting asperity. *Lithos*, 113(1-2), 318-330.
930
- 931 **27.** Fortuin, A. R., Van der Werff, W., & Wensink, H. (1997). Neogene basin history
932 and paleomagnetism of a rifted and inverted forearc region, on- and offshore
933 Sumba, Eastern Indonesia. *Journal of Asian Earth Sciences*, 15(1), 61-88.
934
- 935 **28.** Granger, D. E., & Riebe, C. S. (2014). Cosmogenic nuclides in weathering and
936 erosion.
937
- 938 **29.** Gibb, J. G. (1978). Rates of coastal erosion and accretion in New Zealand. *New
939 Zealand journal of marine and freshwater research*, 12(4), 429-456.
940
- 941 **30.** Gosse, J. C., & Phillips, F. M. (2001). Terrestrial in situ cosmogenic nuclides:
942 theory and application. *Quaternary Science Reviews*, 20(14), 1475-1560.
943
- 944 **31.** Haig, D. W. (2012). Palaeobathymetric gradients across Timor during 5.7-3.3
945 Ma (latest Miocene-Pliocene) and implications for collision uplift.
946 *Palaeogeography, Palaeoclimatology, Palaeoecology*, 331, 50-59.
947

- 948 **32.** Hantoro, W. S., Jouannic, C., & Pirazzoli, P. A. (1989). Terrasses coralliennes
949 quaternaires soulevées dans l'île de Sumba (Indonésie). Photo interprétation
950 (Paris), 28(1), 17-34.
- 951
- 952 **33.** Hantoro, W. S. (1992). Etude des terrasses récifales Quaternaires soulevées
953 entre le Détroit de la Sonde et l'île de Timor, Indonésie: mouvements verticaux
954 de la croûte terrestre et variations du niveau de la mer.
- 955
- 956 **34.** Harris, R. A. (1991). Temporal distribution of strain in the active Banda orogen:
957 a reconciliation of rival hypotheses. *Journal of Southeast Asian Earth Sciences*,
958 6(3-4), 373-386.
- 959
- 960 **35.** Hearty, P. J., & Olson, S. L. (2008). Mega-highstand or megatsunami?
961 Discussion of McMurtry et al. (Elevated marine deposits in Bermuda record a
962 late Quaternary megatsunami: *Sed. Geol.* 200 (2007) 155-165). *Sedimentary*
963 *Geology*, 203(3-4), 307-312.
- 964
- 965 **36.** Hein, A. S., Hulton, N. R. J., Dunai, T. J., Schnabel, C., Kaplan, M. R., Naylor,
966 M., et al. (2009). Middle Pleistocene glaciation in Patagonia dated by
967 cosmogenic-nuclide measurements on outwash gravels. *Earth and Planetary*
968 *Science Letters*, 286(1-2), 184-197.
- 969
- 970 **37.** Heisinger, B., Lal, D., Jull, A. J. T., Kubik, P., Ivy-Ochs, S., Neumaier, S., et al.
971 (2002). Production of selected cosmogenic radionuclides by muons: 1. Fast
972 muons. *Earth and Planetary Science Letters*, 200(3-4), 345-355.

973
974
975
976
977
978
979
980
981
982
983
984
985
986
987
988
989
990
991
992
993
994
995
996
997

38.Hibbert, F. D., Rohling, E. J., Dutton, A., Williams, F. H., Chutcharavan, P. M., Zhao, C., et al. (2016). Coral indicators of past sea-level change: A global repository of U-series dated benchmarks. *Quaternary Science Reviews*, 145, 1-56.

39.Hinschberger, F., Malod, J.-A., Réhault, J.-P., Villeneuve, M., Royer, J.-Y., & Burhanuddin, S. (2005). Late Cenozoic geodynamic evolution of eastern Indonesia. *Tectonophysics*, 404(1-2), 91-118.

40.Hoeksema, B. W. (2012). Extreme morphological plasticity enables a free mode of life in *Favia gravida* at Ascension Island (South Atlantic). *Marine Biodiversity*, 42(2), 289-295.

41.Hopley, D. (2011). Density and porosity: influence on reef accretion rates. In: Springer.

42.Husson, L., Pastier, A.-M., Pedoja, K., Elliot, M., Paillard, D., Authemayou, C., et al. (2018). Reef carbonate productivity during Quaternary sea level oscillations. *Geochemistry, Geophysics, Geosystems*, pp. 1148-1164.

43.James, N. P., & Macintyre, I. G. (1985). Carbonate depositional environments- modern and ancient-Part. 1: Reefs-zonation, depositional facies and diagenesis. *Colorado School of Mines Quarterly*, 80(3).

- 998 **44.**Jouannic, C., Hantoro, W. S., Hoang, C. T., Fournier, M., Lafont, R., & Ichtam,
999 M. L. (1988). Quaternary raised reef terraces at cape Laundi, Sumba,
1000 Indonesia: geomorphological analysis and first radiometric Th/U and ¹⁴C age
1001 determinations. Paper presented at the 6th Proceedings International coral reef
1002 symposium.
- 1003
- 1004 **45.**Kindler, P., Reyss, J.-L., Cazala, C., & Plagnes, V. r. (2007). Discovery of a
1005 composite reefal terrace of middle and late Pleistocene age in Great Inagua
1006 Island, Bahamas. Implications for regional tectonics and sea-level history.
1007 *Sedimentary Geology*, 194(1-2), 141-147.
- 1008
- 1009 **46.**Kummerow, C., Simpson, J., Thiele, O., Barnes, W., Chang, A. T. C., Stocker,
1010 E., et al. (2000). The status of the Tropical Rainfall Measuring Mission (TRMM)
1011 after two years in orbit. *Journal of applied meteorology*, 39(12), 1965-1982.
- 1012
- 1013 **47.**Lal, D. (1988). In situ-produced cosmogenic isotopes in terrestrial rocks. *Annual*
1014 *Review of Earth and Planetary Sciences*, 16(1), 355-388.
- 1015
- 1016 **48.**Lal, D. (1991). Cosmic ray labeling of erosion surfaces: in situ nuclide production
1017 rates and erosion models. *Earth and Planetary Science Letters*, 104(2-4), 424-
1018 439.
- 1019
- 1020 **49.**Lal, D., Gallup, C. D., Somayajulu, B. L. K., Vacher, L. c., Caffee, M. W., Jull, A.
1021 J. T., et al. (2005). Records of cosmogenic radionuclides ¹⁰Be, ²⁶Al and ³⁶Cl

- 1022 in corals: First studies on coral erosion rates and potential of dating very old
1023 corals. *Geochimica et cosmochimica acta*, 69(24), 5717-5728.
- 1024
- 1025 **50.**Levenson, Y., Ryb, U., & Emmanuel, S. (2017). Comparison of field and
1026 laboratory weathering rates in carbonate rocks from an Eastern Mediterranean
1027 drainage basin. *Earth and Planetary Science Letters*, 465, 176-183.
- 1028
- 1029 **51.**Liew, P.-M., & Hsieh, M.-L. (2000). Late Holocene (2 ka) sea level, river
1030 discharge and climate interrelationship in the Taiwan region. *Journal of Asian*
1031 *Earth Sciences*, 18(4), 499-505.
- 1032
- 1033 **52.**Lundberg, J. (2019). Karren, surface. In *Encyclopedia of Caves* (pp. 600-608):
1034 Elsevier.
- 1035
- 1036 **53.**Merchel, S., Arnold, M., Aumaître, G., Benedetti, L., Bourlès, D. L., Braucher,
1037 R., et al. (2008). Towards more precise ^{10}Be and ^{36}Cl data from measurements
1038 at the 10-14 level: influence of sample preparation. *Nuclear instruments and*
1039 *methods in physics research section B: beam interactions with materials and*
1040 *atoms*, 266(22), 4921-4926.
- 1041
- 1042 **54.**Muhs, D. R. (2001). Evolution of soils on Quaternary reef terraces of Barbados,
1043 West Indies. *Quaternary research*, 56(1), 66-78.
- 1044
- 1045 **55.**Murray-Wallace, C. V., & Woodroffe, C. D. (2014). *Quaternary sea-level*
1046 *changes: a global perspective*: Cambridge University Press.

1047

1048 **56.**Nexer, M., Authemayou, C., Schildgen, T., Hantoro, W. S., Molliex, S.,
1049 Delcaillau, B., et al. (2015). Evaluation of morphometric proxies for uplift on
1050 sequences of coral reef terraces: A case study from Sumba Island (Indonesia).
1051 *Geomorphology*, 241, 145-159.

1052

1053 **57.**Nugroho, H., Harris, R., Lestariya, A. W., & Maruf, B. (2009). Plate boundary
1054 reorganization in the active Banda Arc-continent collision: Insights from new
1055 GPS measurements. *Tectonophysics*, 479(1-2), 52-65.

1056

1057 **58.**Obert, J. C., Scholz, D., Felis, T., Brocas, W. M., Jochum, K. P., & Andreae, M.
1058 O. (2016). $^{230}\text{Th}/\text{U}$ dating of Last Interglacial brain corals from Bonaire
1059 (southern Caribbean) using bulk and theca wall material. *Geochimica et*
1060 *cosmochimica acta*, 178, 20-40.

1061

1062 **59.**Obert, J. C., Scholz, D., Felis, T., Lippold, J., Jochum, K. P., & Andreae, M. O.
1063 (2019). Improved constraints on open-system processes in fossil reef corals by
1064 combined Th/U, Pa/U and Ra/Th dating: A case study from Aqaba, Jordan.
1065 *Geochimica et cosmochimica acta*, 245, 459-478.

1066

1067 **60.** Orr, Y., Schimmer, R., Geerken, R., Castro, A., Taylor, D., & Brokensha, D.
1068 (2012). Ethno-ecology in the shadow of rain and the light of experience: local
1069 perceptions of drought and climate change in east Sumba, Indonesia. *Climate*
1070 *Change and Threatened Communities* [Castro, AP, D. Taylor, and DW
1071 Brokensha (eds.)]. Practical Action Publishing, Rugby, UK, 175-184.

1072

1073 **61.**Pastier, A. M., Husson, L., Pedoja, K., Bézos, A., Authemayou, C., Arias-Ruiz,
1074 C., et al. (2019). Genesis and Architecture of Sequences of Quaternary Coral
1075 Reef Terraces: Insights From Numerical Models. *Geochemistry, Geophysics,*
1076 *Geosystems.*

1077

1078 **62.**Pedoja, K., Husson, L., Regard, V., Cobbold, P. R., Ostanciaux, E., Johnson,
1079 M. E., et al. (2011). Relative sea-level fall since the last interglacial stage: are
1080 coasts uplifting worldwide? *Earth-Science Reviews*, 108(1-2), 1-15.

1081

1082 **63.**Pedoja, K., Husson, L., Johnson, M. E., Melnick, D., Witt, C., Pochat, S. p., et
1083 al. (2014). Coastal staircase sequences reflecting sea-level oscillations and
1084 tectonic uplift during the Quaternary and Neogene. *Earth-Science Reviews*,
1085 132, 13-38.

1086

1087 **64.**Pedoja, K., Husson, L., Bézos, A., Pastier, A.-M., Imran, A. M., Arias-Ruiz, C.,
1088 et al. (2018). On the long-lasting sequences of coral reef terraces from SE
1089 Sulawesi (Indonesia): Distribution, formation, and global significance.
1090 *Quaternary Science Reviews*, 188, 37-57.

1091

1092 **65.**Phillips, F. M., & Plummer, M. A. (1996). CHLOE; a program for interpreting in-
1093 situ cosmogenic nuclide data for surface exposure dating and erosion studies.
1094 *Radiocarbon*, 38(1), 98-99.

1095

- 1096 **66.**Phillips, F. M., Stone, W. D., & Fabryka-Martin, J. T. (2001). An improved
1097 approach to calculating low-energy cosmic-ray neutron fluxes near the
1098 land/atmosphere interface. *Chemical Geology*, 175(3-4), 689-701.
1099
- 1100 **67.**Pirazzoli, P. A., Radtke, U., Hantoro, W. S., Jouannic, C., Hoang, C. T., Causse,
1101 C., et al. (1991). Quaternary raised coral-reef terraces on Sumba Island,
1102 Indonesia. *Science*, 252(5014), 1834-1836.
1103
- 1104 **68.**Pirazzoli, P. A., Radtke, U., Hantoro, W. S., Jouannic, C., Hoang, C. T., Causse,
1105 C., et al. (1993). A one million-year-long sequence of marine terraces on Sumba
1106 Island, Indonesia. *Marine Geology*, 109(3-4), 221-236.
1107
- 1108 **69.**Pirazzoli, P. A. (2005). A review of possible eustatic, isostatic and tectonic
1109 contributions in eight late-Holocene relative sea-level histories from the
1110 Mediterranean area. *Quaternary Science Reviews*, 24(18-19), 1989-2001.
1111
- 1112 **70.**Prasetia, R., As-syakur, A. R., & Osawa, T. (2013). Validation of TRMM
1113 Precipitation Radar satellite data over Indonesian region. *Theoretical and
1114 applied climatology*, 112(3-4), 575-587.
1115
- 1116 **71.**Raimbault, C., Duperret, A., Regard, V., Molliex, S., Wyns, R., Authemayou, C.,
1117 et al. (2018). Quaternary geomorphological evolution of a granitic shore platform
1118 constrained by in situ ¹⁰Be concentrations, Penmarc'h, SW Brittany, France.
1119 *Marine Geology*, 395, 33-47.
1120

- 1121 **72.**Rasser, M., & Riegl, B. (2002). Holocene coral reef rubble and its binding
1122 agents. *Coral Reefs*, 21(1), 57-72.
1123
- 1124 **73.**Regard, V., Dewez, T., Bourles, D. L., Anderson, R. S., Duperret, A., Costa, S.,
1125 et al. (2012). Late Holocene seacliff retreat recorded by 10Be profiles across a
1126 coastal platform: Theory and example from the English Channel. *Quaternary*
1127 *Geochronology*, 11, 87-97.
1128
- 1129 **74.**Rovere, A., Raymo, M. E., Vacchi, M., Lorscheid, T., Stocchi, P., Gomez-Pujol,
1130 L., et al. (2016). The analysis of Last Interglacial (MIS 5e) relative sea-level
1131 indicators: Reconstructing sea-level in a warmer world. *Earth-Science Reviews*,
1132 159, 404-427.
1133
- 1134 **75.**Rupnik, E., Deseilligny, M. P., Delorme, A., & Klinger, Y. (2016). Refined
1135 satellite image orientation in the free open-source photogrammetric tools
1136 Apero/Micmac. *ISPRS Annals of the Photogrammetry, Remote Sensing and*
1137 *Spatial Information Sciences*, 3, 83.
1138
- 1139 **76.**Russell-Smith, J., Djoeroemana, S., Maan, J., & Pandanga, P. (2007). Rural
1140 livelihoods and burning practices in savanna landscapes of Nusa Tenggara
1141 Timur, eastern Indonesia. *Human Ecology*, 35(3), 345-359.
1142
- 1143 **77.**Ryb, U., Matmon, A., Erel, Y., Haviv, I., Benedetti, L., & Hidy, A. J. (2014). Styles
1144 and rates of long-term denudation in carbonate terrains under a Mediterranean

1145 to hyper-arid climatic gradient. *Earth and Planetary Science Letters*, 406, 142-
1146 152.

1147

1148 **78.**Schaller, M., Ehlers, T. A., Blum, J. D., & Kallenberg, M. A. (2009). Quantifying
1149 glacial moraine age, denudation, and soil mixing with cosmogenic nuclide depth
1150 profiles. *Journal of Geophysical Research: Earth Surface*, 114(F1).

1151

1152 **79.**Schimmelpfennig, I., Benedetti, L., Finkel, R., Pik, R. I., Blard, P.-H., Bourles,
1153 D., et al. (2009). Sources of in-situ ³⁶Cl in basaltic rocks. Implications for
1154 calibration of production rates. *Quaternary Geochronology*, 4(6), 441-461.

1155

1156 **80.**Schimmelpfennig, I., Benedetti, L., Garreta, V., Pik, R., Blard, P.-H., Burnard,
1157 P., et al. (2011). Calibration of cosmogenic ³⁶Cl production rates from Ca and
1158 K spallation in lava flows from Mt. Etna (38 N, Italy) and Payun Matru (36 S,
1159 Argentina). *Geochimica et cosmochimica acta*, 75(10), 2611-2632.

1160

1161 **81.**Schimmelpfennig, I., Schaefer, J. M., Putnam, A. E., Koffman, T., Benedetti, L.,
1162 Ivy-Ochs, S., et al. (2014). ³⁶Cl production rate from K-spallation in the
1163 European Alps (Chironico landslide, Switzerland). *Journal of Quaternary
1164 Science*, 29(5), 407-413.

1165

1166 **82.**Schlagenhauf, A., Gaudemer, Y., Benedetti, L., Manighetti, I., Palumbo, L.,
1167 Schimmelpfennig, I., et al. (2010). Using in situ Chlorine-36 cosmonuclide to
1168 recover past earthquake histories on limestone normal fault scarps: a

1169 reappraisal of methodology and interpretations. *Geophysical Journal*
1170 *International*, 182(1), 36-72.

1171

1172 **83.**Scholz, D., Mangini, A., & Felis, T. (2004). U-series dating of diagenetically
1173 altered fossil reef corals. *Earth and Planetary Science Letters*, 218(1-2), 163-
1174 178.

1175

1176 **84.**Schwartz, M. (2006). *Encyclopedia of coastal science*: Springer Science &
1177 Business Media.

1178

1179 **85.**Scoffin, T. P. (1993). The geological effects of hurricanes on coral reefs and the
1180 interpretation of storm deposits. *Coral Reefs*, 12(3-4), 203-221.

1181

1182 **86.**Shekeine, J., Turnbull, L. A., Cherubini, P., de Jong, R., Baxter, R., Hansen, D.,
1183 et al. (2015). Primary productivity and its correlation with rainfall on Aldabra
1184 Atoll. *Biogeosciences Discussions*, 12(2), 981-1013.

1185

1186 **87.**Simms, A. R. (2021). Last interglacial sea levels within the Gulf of Mexico and
1187 northwestern Caribbean Sea. *Earth System Science Data*, 13(3), 1419-1439.

1188

1189 **88.**Smith, S. V. (1983). Coral reef calcification. *Perspectives on Coral Reefs*.
1190 Australian Institute of Marine Science, 240-247.

1191

- 1192 **89.**Speed, R. C., & Cheng, H. (2004). Evolution of marine terraces and sea level in
1193 the last interglacial, Cave Hill, Barbados. *Geological Society of America Bulletin*,
1194 116(1-2), 219-232.
- 1195
- 1196 **90.**Spencer, T. (1985). Weathering rates on a Caribbean reef limestone: results
1197 and implications. *Marine Geology*, 69(1-2), 195-201.
- 1198
- 1199 **91.**Stephenson, W. J., & Kirk, R. M. (1998). Rates and patterns of erosion on inter-
1200 tidal shore platforms, Kaikoura Peninsula, South Island, New Zealand. *Earth*
1201 *Surface Processes and Landforms: The Journal of the British Geomorphological*
1202 *Group*, 23(12), 1071-1085.
- 1203
- 1204 **92.**Stone, J., Allan, G. L., Fifield, L. K., Evans, J. M., & Chivas, A. R. (1994).
1205 Limestone erosion measurements with cosmogenic chlorine-36 in calcite-
1206 preliminary results from Australia. *Nuclear instruments and methods in physics*
1207 *research section B: beam interactions with materials and atoms*, 92(1-4), 311-
1208 316
- 1209
- 1210 **93.**Stone, J. O., Allan, G. L., Fifield, L. K., & Cresswell, R. G. (1996). Cosmogenic
1211 chlorine-36 from calcium spallation. *Geochimica et cosmochimica acta*, 60(4),
1212 679-692.
- 1213
- 1214 **94.**Stone, J. O. H., Evans, J. M., Fifield, L. K., Allan, G. L., & Cresswell, R. G.
1215 (1998). Cosmogenic chlorine-36 production in calcite by muons. *Geochimica et*
1216 *cosmochimica acta*, 62(3), 433-454.

1217

1218 **95.** Tate, G. W., McQuarrie, N., Van Hinsbergen, D. J. J., Bakker, R. R., Harris, R.,
1219 Willett, S., et al. (2014). Resolving spatial heterogeneities in exhumation and
1220 surface uplift in Timor-Leste: Constraints on deformation processes in young
1221 orogens. *Tectonics*, 33(6), 1089-1112.

1222

1223 **96.** Thompson, S. B., & Creveling, J. R. (2021). A Global Database of Marine
1224 Isotope Stage 5a and 5c Marine Terraces and Paleoshoreline Indicators. *Earth*
1225 *System Science Data Discussions*, 1-32.

1226

1227 **97.** Trudgill, S. T. (1976). The marine erosion of limestones on Aldabra Atoll, Indian
1228 Ocean. *Zeitschrift für Geomorphologie*, 26, 164-200.

1229

1230 **98.** Trudgill, S. T. (1979). Surface lowering and landform evolution on Aldabra.
1231 *Philosophical Transactions of the Royal Society of London. B, Biological*
1232 *Sciences*, 286(1011), 35-45.

1233

1234 **99.** Van der Werff, W. (1995). Cenozoic evolution of the Savu Basin, Indonesia:
1235 forearc basin response to arc-continent collision. *Marine and Petroleum*
1236 *Geology*, 12(3), 247-262.

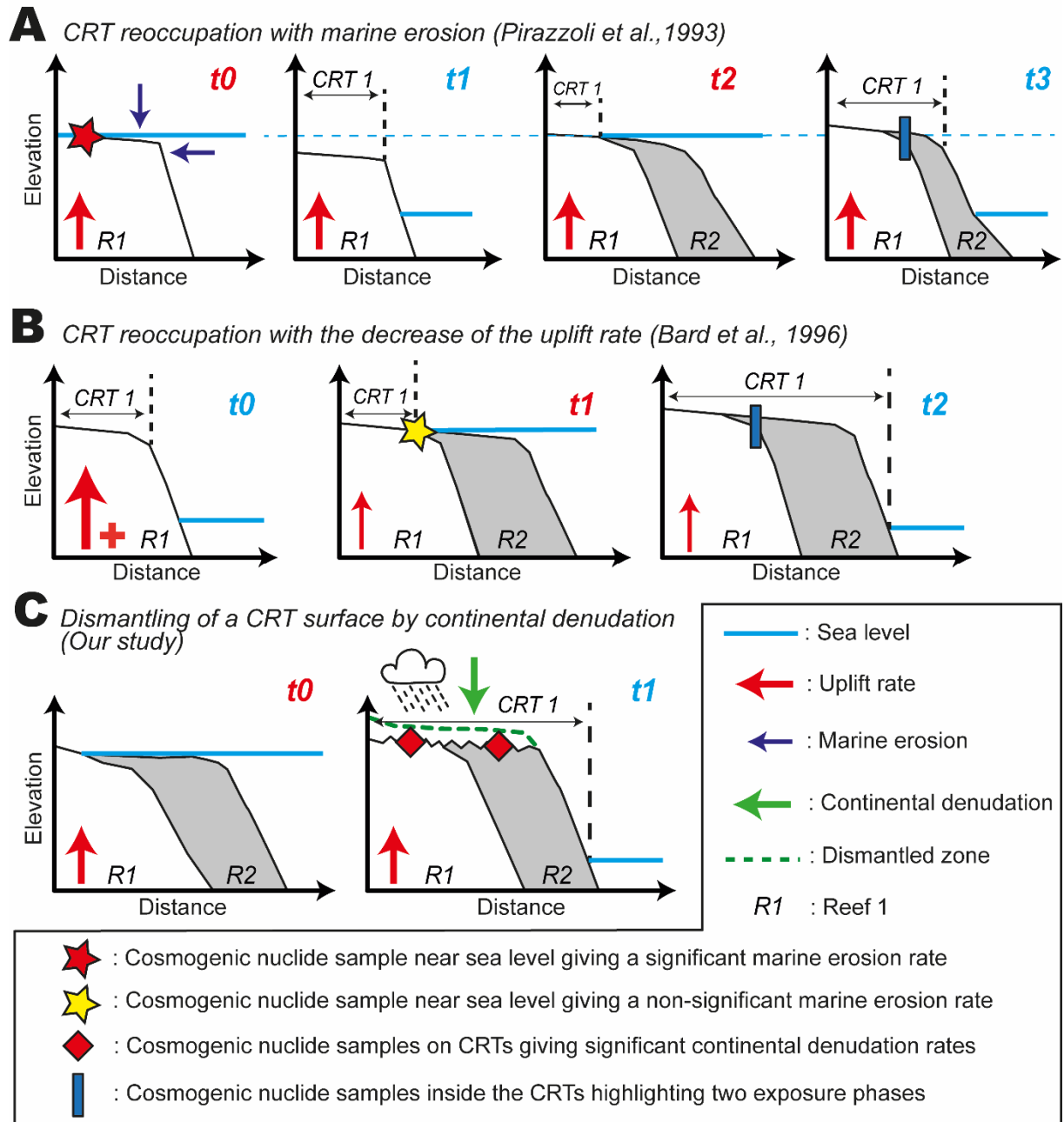
1237

1238 **100.** Vasconcelos, P. M. D., & Stone, J. O. (2000). Studies of geomorphic
1239 rates and processes with cosmogenic isotopes-examples from Australia.

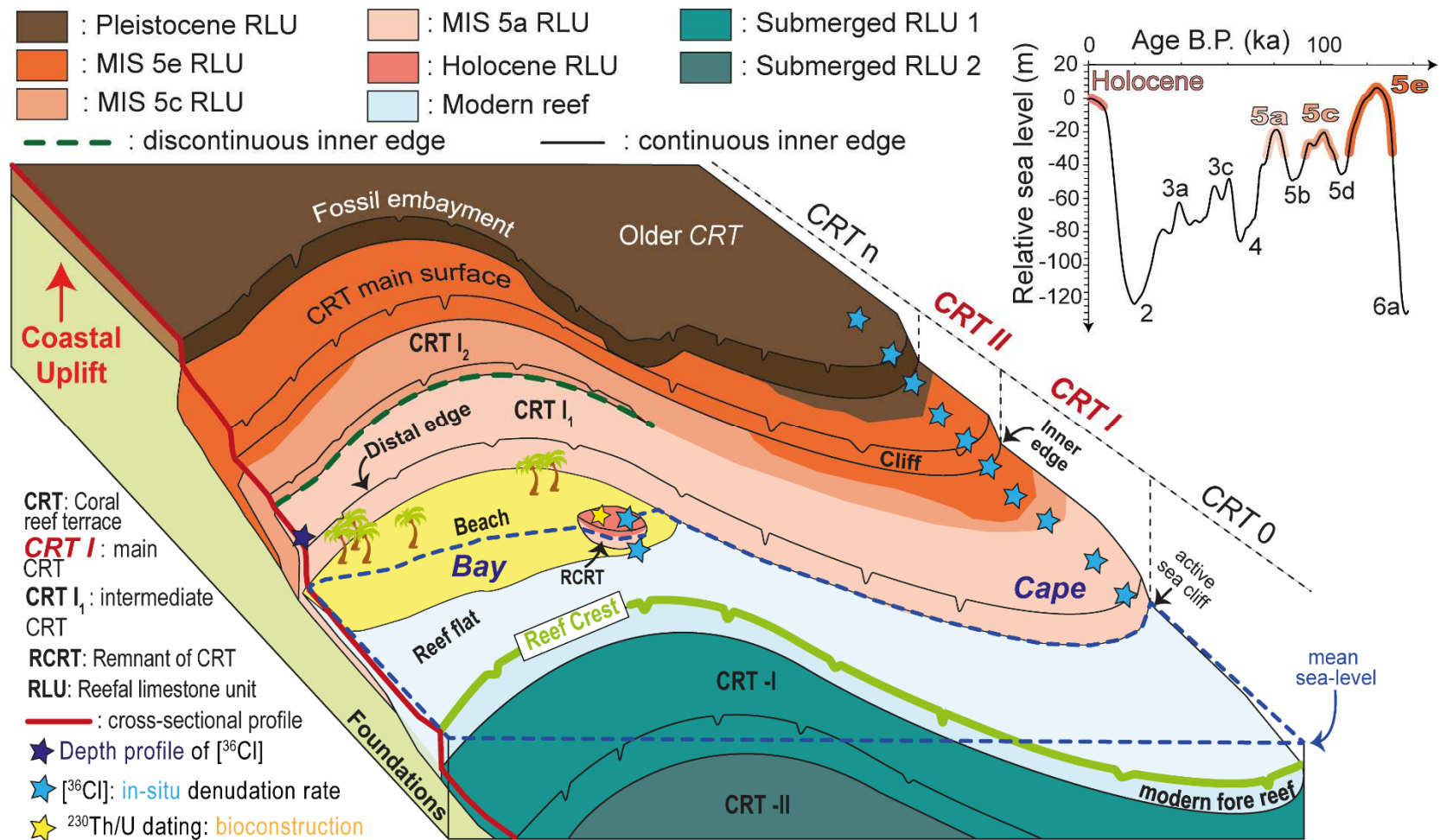
1240

- 1241 **101.** Vermeesch, P. (2007). CosmoCalc: An Excel add-in for cosmogenic
1242 nuclide calculations. *Geochemistry, Geophysics, Geosystems*, 8(8).
1243
- 1244 **102.** Von Blanckenburg, F. (2005). The control mechanisms of erosion and
1245 weathering at basin scale from cosmogenic nuclides in river sediment. *Earth
1246 and Planetary Science Letters*, 242(3-4), 224-239.
1247
- 1248 **103.** Von der Borch, C. C., Grady, A. E., Hardjoprawiro, S., Prasetyo, H., &
1249 Hadiwisastra, S. (1983). Mesozoic and late Tertiary submarine fan sequences
1250 and their tectonic significance, Sumba, Indonesia. *Sedimentary Geology*, 37(1-
1251 2), 113-132.
1252
- 1253 **104.** Waelbroeck, C., Labeyrie, L., Michel, E., Duplessy, J. C., McManus, J.
1254 F., Lambeck, K., et al. (2002). Sea-level and deep water temperature changes
1255 derived from benthic foraminifera isotopic records. *Quaternary Science
1256 Reviews*, 21(1-3), 295-305.
1257
- 1258 **105.** Yang, Q., Scholz, D., Jochum, K. P., Hoffmann, D. L., Stoll, B., Weis, U.,
1259 et al. (2015). Lead isotope variability in speleothems-A promising new proxy for
1260 hydrological change? First results from a stalagmite from western Germany.
1261 *Chemical Geology*, 396, 143-151.
1262
1263
1264

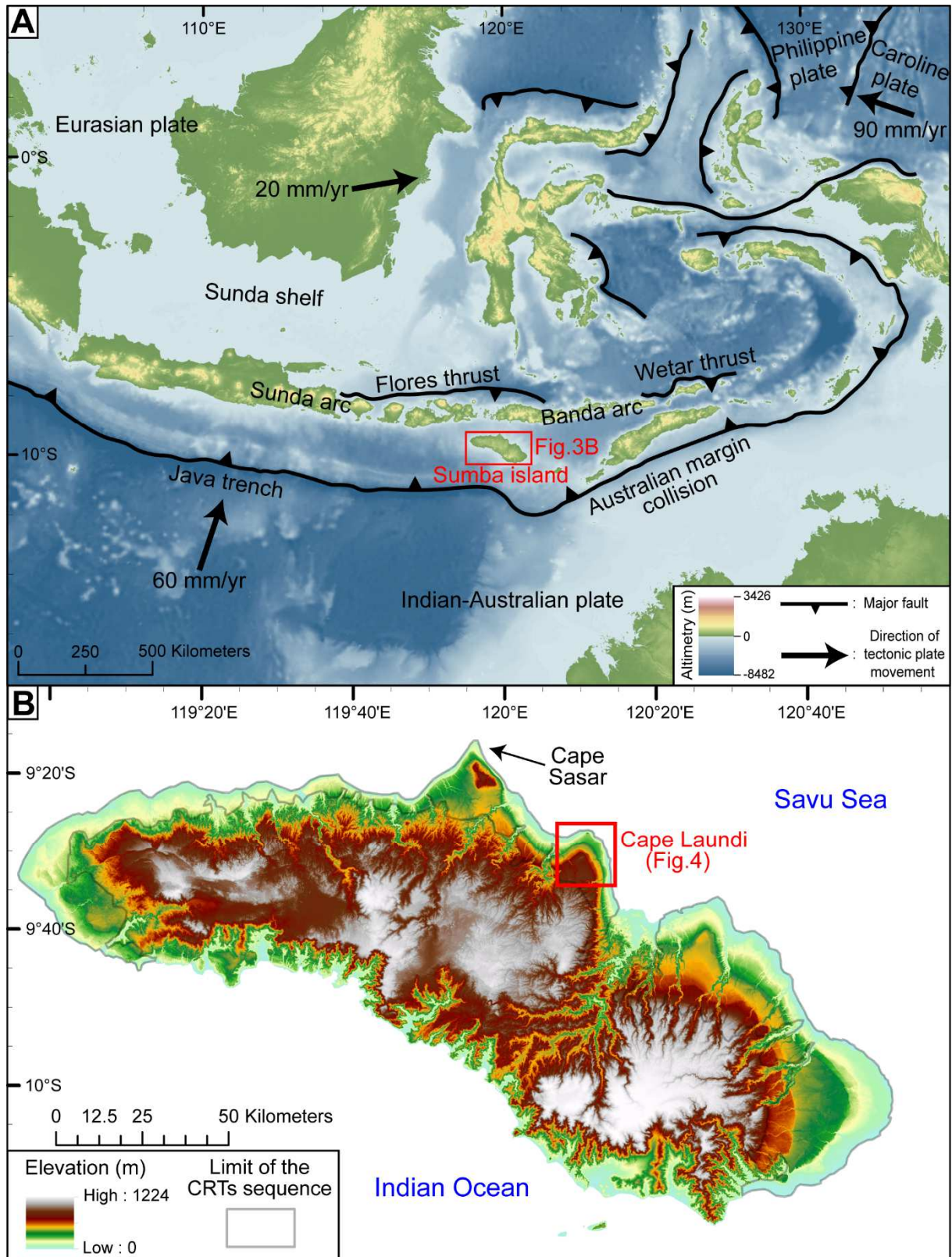
Figures



1267 **Fig. 1.** Three hypotheses explaining diachronous ages on the same surface of the
1268 Cape Laundi CRTs. **A)** Important role of marine erosion in the destruction of the
1269 emergent CRTs, helping a later reoccupation of these eroded surfaces (Pirazzoli et al.,
1270 1993). **B)** The decrease in the rate of uplift to a low rate (about 0.2 mm a^{-1}) promotes
1271 the reoccupation of emergent CRTs without marine erosion (Bard et al., 1996). **C)**
1272 Alternative hypothesis (this study): continental denudation may partially dismantle
1273 emergent surfaces, generating a diachronism of these surfaces. ^{36}Cl cosmogenic
1274 data on CRT near current sea level reveal the significance of marine erosion (Fig. 1A)
1275 and continental denudation (Fig. 1C).



1276 **Fig. 2.** Schematic plot of a sequence of coral reef terraces, modified from Pedoja et al. (2018). The blue and yellow stars represent
 1277 the location of samples collected on the CRT surfaces and intended for analysis in ³⁶Cl concentration and ²³⁰Th/U dating, respectively.
 1278 The relative sea level curve is from Waelbroeck et al. (2002).

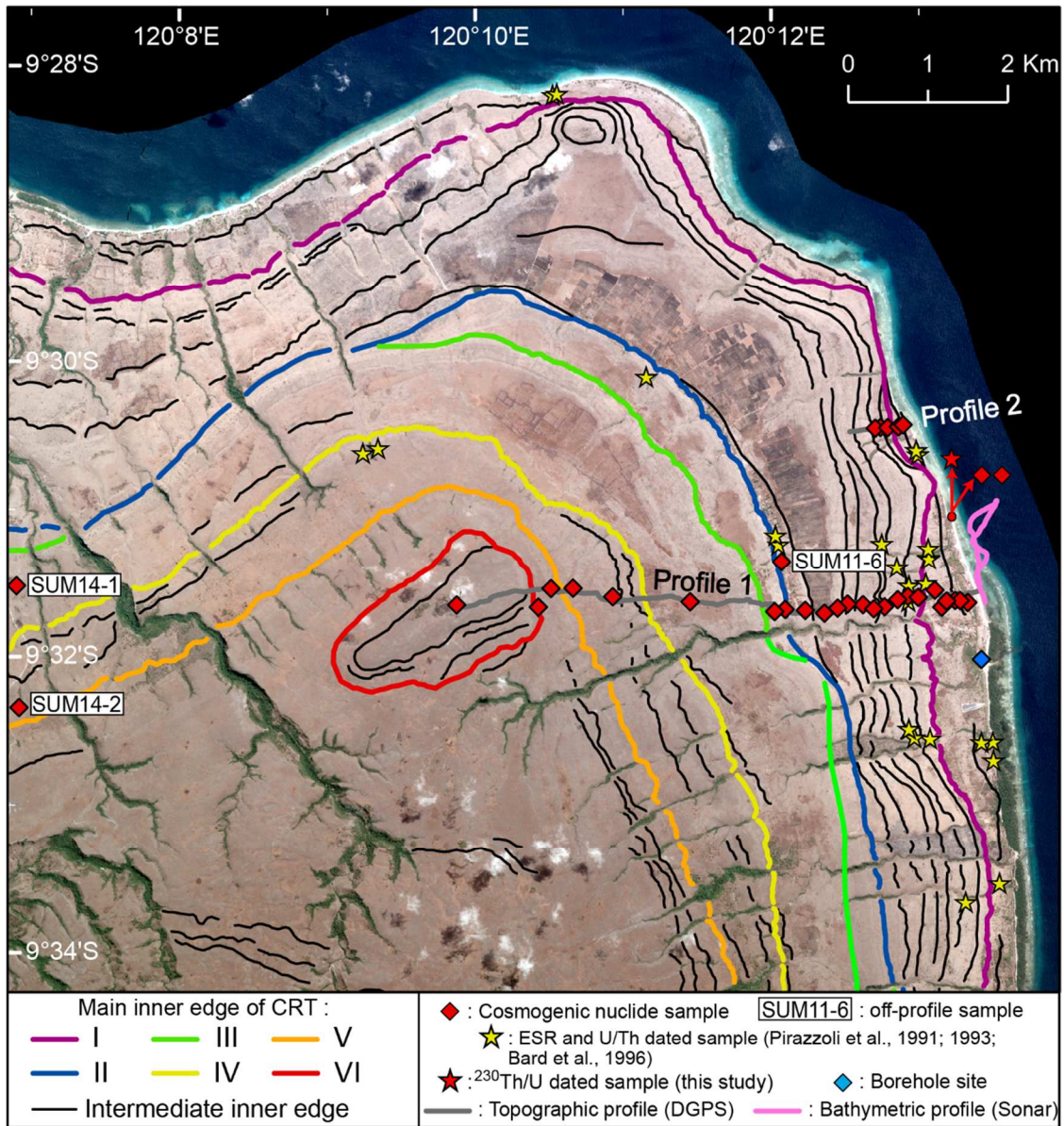


1279 **Fig. 3. A)** Geodynamics of SE Asia and location of Sumba Island (Indonesia). Plate
 1280 velocities indicated in relation to the Eurasia plate, from Nugroho et al. (2009),
 1281 elevation data from the Shuttle Radar Topography Mission (SRTM), and bathymetry

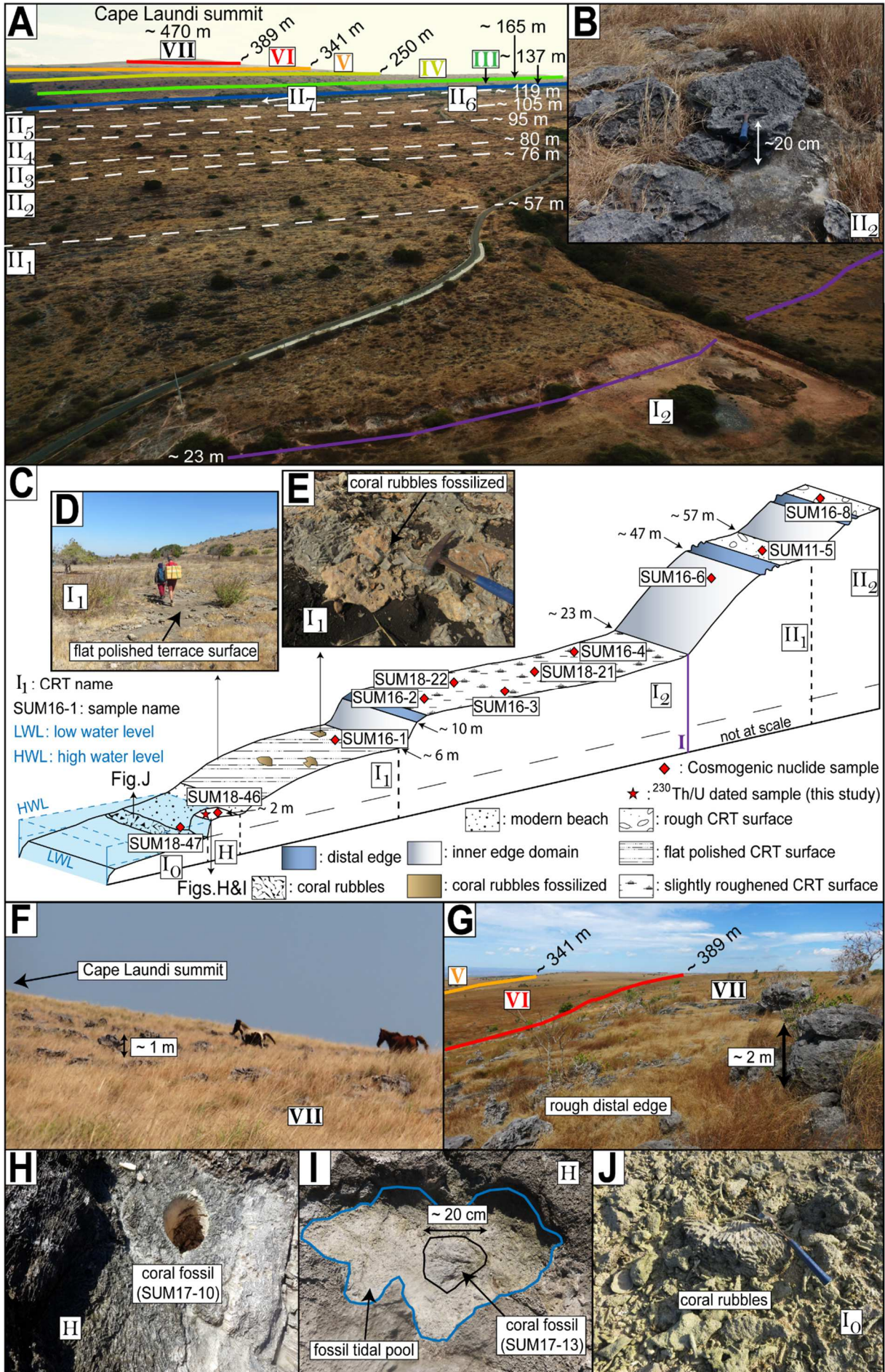
1282 data from the General Bathymetric Chart of Oceans (GEBCO), both at 90 m resolution.

1283 **B)** Digital elevation model (TanDEM-X, 13 m resolution) of Sumba Island.

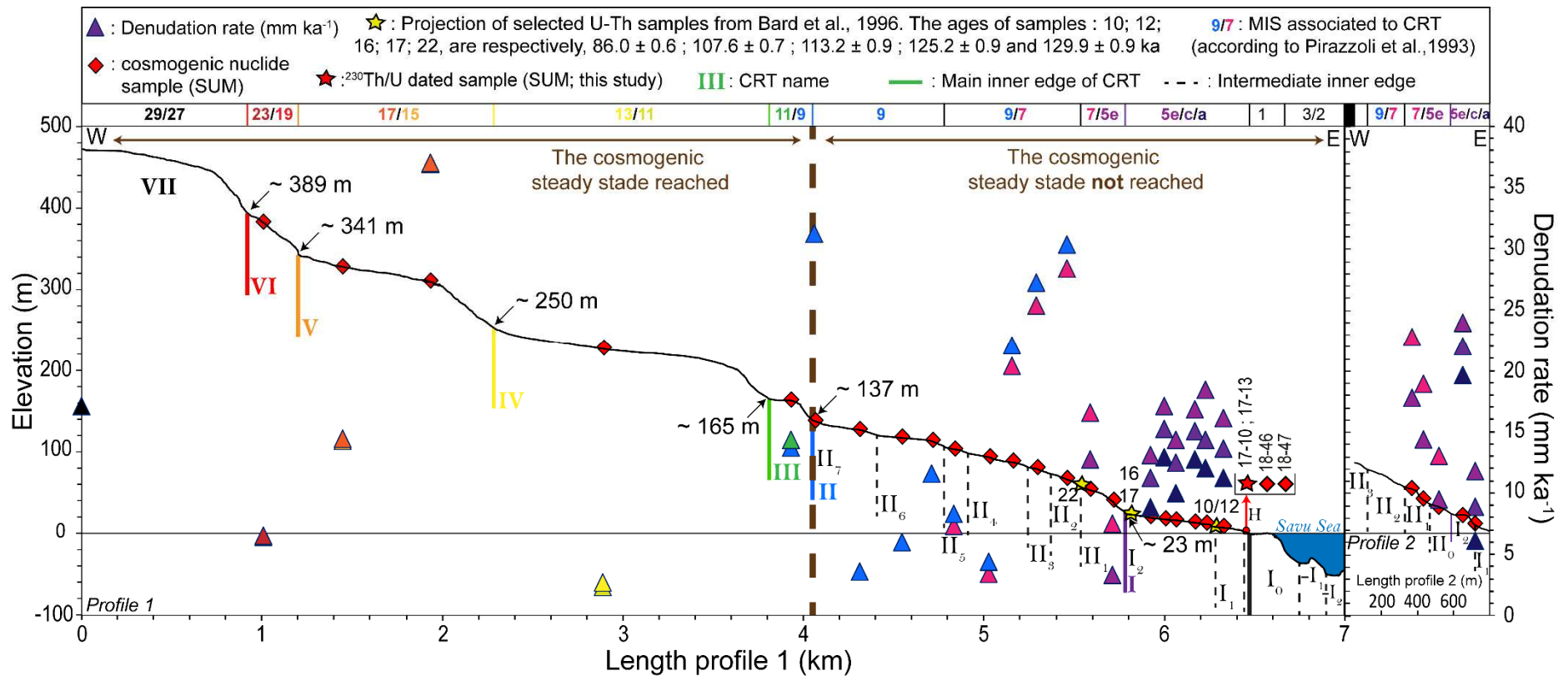
1284



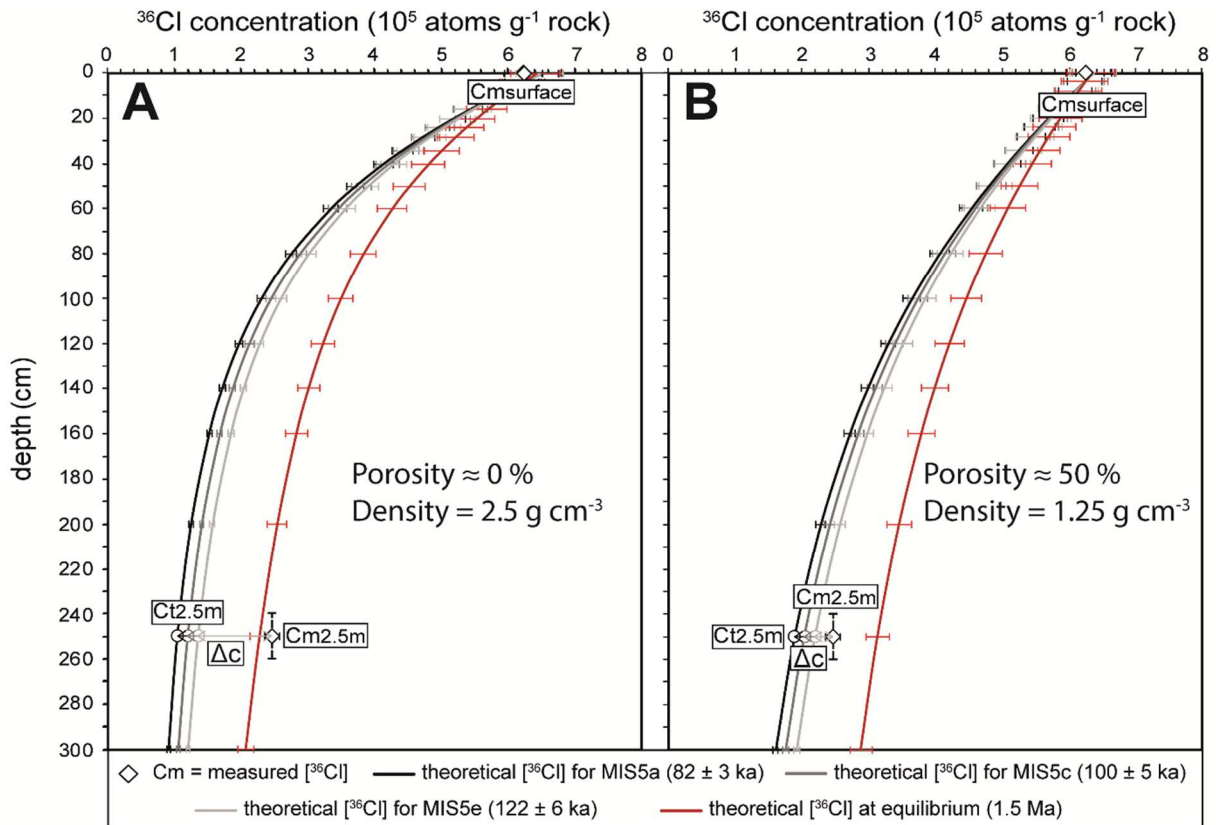
1285 **Fig. 4.** CRTs inner edges of the Cape Laundi sequence (Pleiades satellite imagery, 1
 1286 m resolution), and the location of samples, topographic and bathymetric profiles.



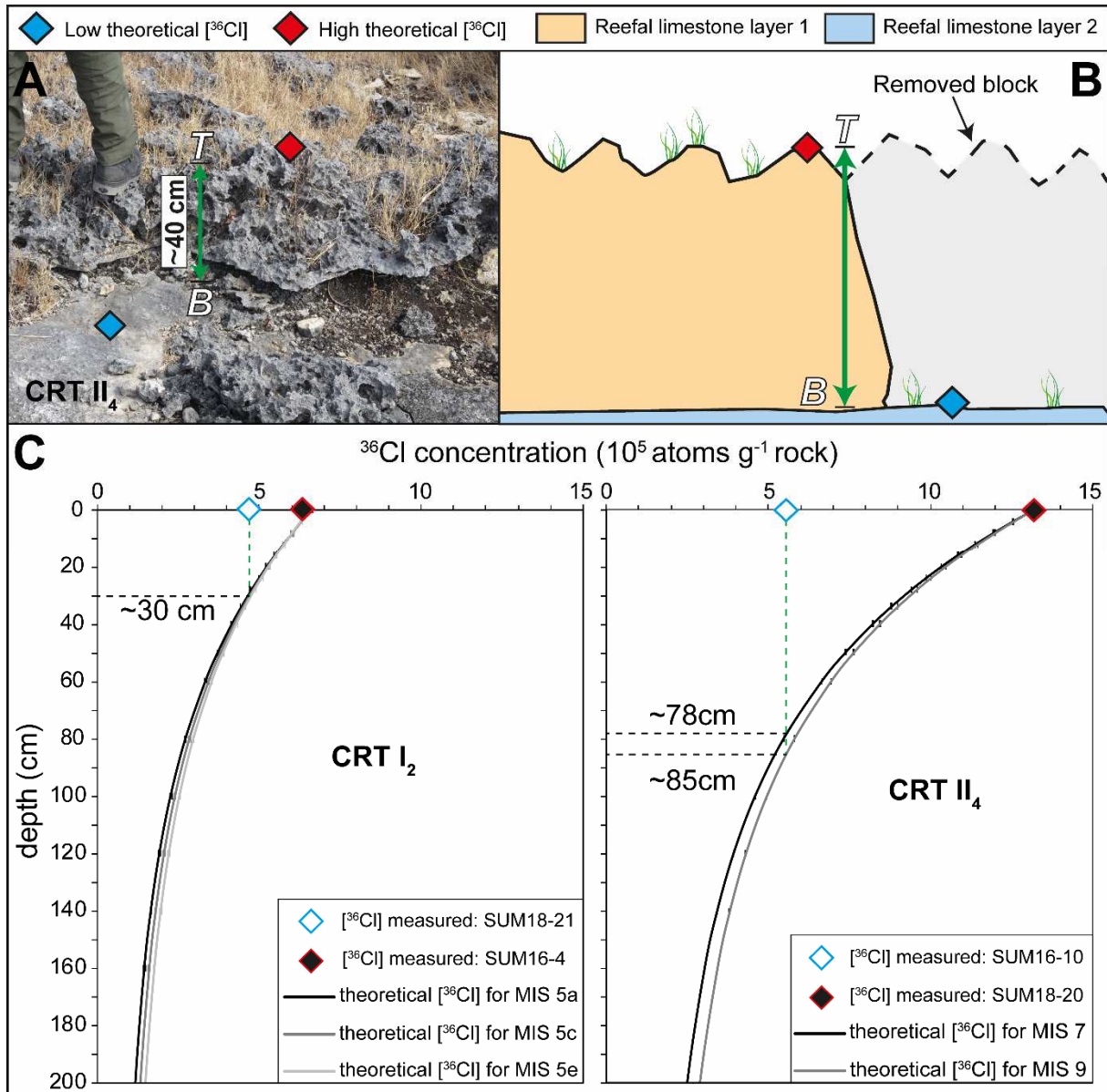
1288 **Fig. 5.** Pictures and interpretations of the Cap Laundi CRTs sequence. The elevations
1289 result from the DGPS profile. **A)** Aerial photo of Cape Laundi showing the staircase
1290 coastal landscape. **B)** CRT II₂ surface. **C)** Schematic 3D diagram of the lowest CRTs,
1291 with locations of Figs. 5D; 5E; 5H; 5I; 5J. **D)** Smooth flat surface of CRT I₁. **E)** Fossil
1292 coral rubbles cemented within the reefal limestones outcropping on the CRT I₁ surface.
1293 **F)** Cape Laundi summit. **G)** Distal edge of CRT VII. **H)** Sample SUM17-10. **I)** Sample
1294 SUM17-13). **J)** Coral rubbles on the modern reef flat (CRT I₀).



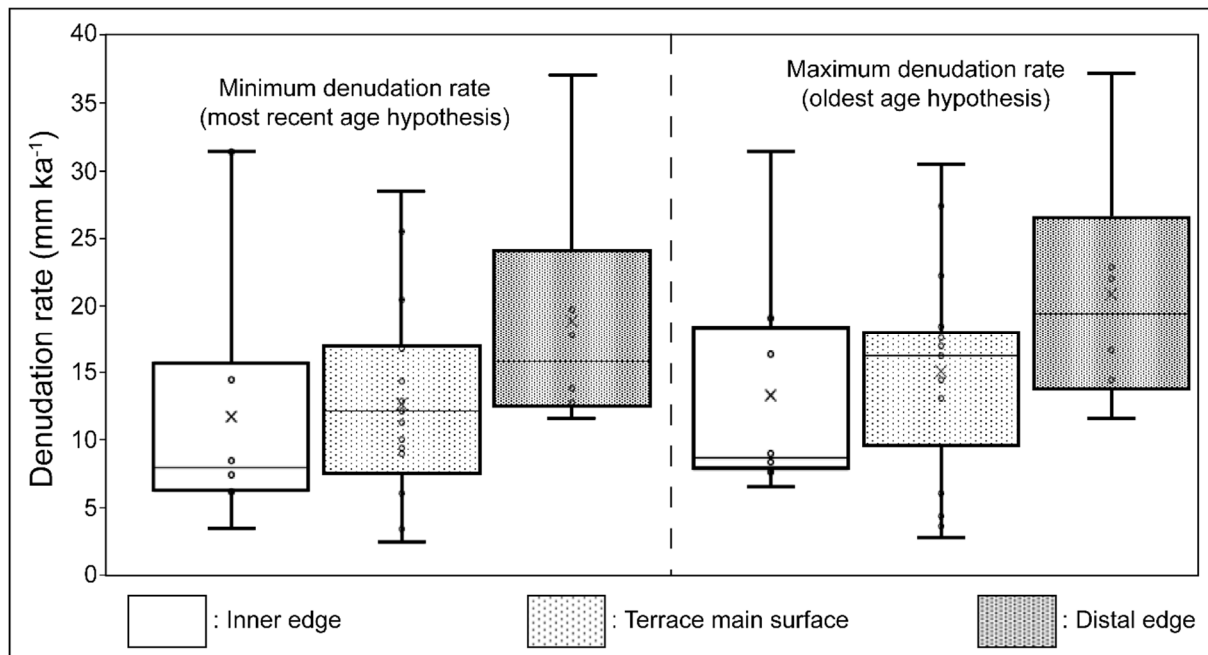
1295 **Fig. 6.** Altimetric profiles (DGPS and sonar) at Cape Laundi, showing the calculated denudation rates with various age hypotheses
 1296 (the colors of the triangles correspond to different age hypotheses), as well as location and ages of U/Th samples (Bard et al., 1996;
 1297 this study).



1298 **Fig. 7.** Surface ($C_{m\text{surface}}$) and $2.5 \pm 0.1 \text{ m}$ ($C_{m2.5m}$) depth ^{36}Cl concentration of the
 1299 borehole within CRT I_1 for a porosity of **A**) 50 % (i.e., density = 1.25 g cm^{-3}) and **B**) 0%
 1300 (density = 2.5 g cm^{-3}). Theoretical ^{36}Cl concentration curves as a function of depth and
 1301 MIS and age hypotheses. ΔC is the difference between measured ^{36}Cl ($C_{m2.5m}$) and
 1302 theoretical concentrations at $2.5 \pm 0.1 \text{ m}$ depth ($C_{t2.5m}$).



1303 **Fig. 8.** ^{36}Cl concentration variations at the scale of a CRT. **A)** Epikarstification on the
 1304 surface of CRT II₄. **B)** Schematic cross-sectional view of Figure 7A. *T* and *B*
 1305 correspond to the top and bottom of the reefal limestone layer 1, respectively. **C)**
 1306 Theoretical ^{36}Cl concentration curves of depth for 2 samples pairs (SUM18-21/16-4
 1307 and SUM18-20/16-10) as a function of depth and MIS and age hypotheses, assuming
 1308 that the ages of reefal bioconstruction and exposure duration are synchronous, as
 1309 proposed by Pirazzoli et al. (1991; 1993).



1310 **Fig. 9.** Boxplots of denudation rates, calculated with the most recent and oldest age
 1311 hypothesis, classified by morphological zone. The crosses, inner bars, circles, upper,
 1312 and lower outer bars represent the average, median, data, maximum and minimum
 1313 value for ³⁶Cl concentrations, respectively.

1314

1315 **Tables**

Sample (SUM)	Sample information						Sample composition		²³⁰ Th/U chemistry							
	Coral species	CRT	Morphology location	Longitude (E)	Latitude (N)	Elevation (m)	Calcite (%)	Aragonite (%)	²³⁸ U (μg/g)	²³² Th (ng/g)	(²³⁴ U/ ²³⁸ U)	(²³⁰ Th/ ²³⁸ U)	age uncorrected (ka)	age corrected (ka)	MIS	(²³⁴ U/ ²³⁸ U)initial
17-10	<i>Pseudodiploria clivosa</i>	H	Distal edge	120.221	-9.52	2.0 ± 0.5	< 1	> 99	2.37 ± 0.01	1.080 ± 0.006	1.14627 ± 0.00041	0.05584 ± 0.00020	5.460 ± 0.020	5.448 ± 0.02	1	1.14854 ± 0.00040
17-13	<i>Mussismilia leptophylla</i>	H	Distal edge	120.221	-9.52	2.0 ± 0.5	< 1	> 99	3.02 ± 0.02	1.281 ± 0.007	1.1404 ± 0.0003	0.02199 ± 0.00010	2.1359 ± 0.0083	2.1252 ± 0.0098	1	1.14126 ± 0.00030

1316 **Table 1.** Results of ²³⁰Th/U dating of samples SUM17-10 and SUM17-13.

1317

1318

1319

1320

1321

1322

1323

1324

1325

1326

1327

1328

1329

Sample (SUM)	Sample location, elevation, slope and Mean Annual Precipitation (MAP)							Sample composition			AMS result
	DGPS profile	CRT name	Longitude (E)	Latitude (N)	Elevation (m)	Slope (°)	MAP (mm yr ⁻¹)	Cl (target fraction) (ppm ± 0.12)	CaO (target fraction) (wt% ± 0.25)	MgO (bulk rock) (wt%)	[³⁶ Cl] (10 ⁵ atom g ⁻¹ rock)
16-1	Profile 1	I1	120.2222	-9.5272	8.4 ± 0.5	0.0	722.8	26.23	55.24	0.39	5.95 ± 0.14
16-2	Profile 1	I2	120.2213	-9.5270	12.5 ± 0.5	2.6	722.3	15.08	54.82	0.47	5.43 ± 0.13
18-22	Profile 1	I2	120.2208	-9.5270	14.4 ± 0.5	1.5	723.3	14.17	52.06	0.57	4.82 ± 0.11
16-3	Profile 1	I2	120.2198	-9.5271	17.4 ± 0.5	3.8	727.3	12.26	56.61	0.36	6.1 ± 0.14
18-21	Profile 1	I2	120.2193	-9.5278	18.5 ± 0.5	1.5	739.9	6.29	54.34	0.32	4.69 ± 0.10
16-4	Profile 1	I2	120.2185	-9.5258	20.4 ± 0.5	1.7	723.9	14.94	55.77	0.29	6.26 ± 0.14
16-6	Profile 1	II1	120.2166	-9.5266	40.7 ± 0.5	14.9	750.7	3.07	55.80	0.34	9.7 ± 0.22
11-5	Profile 1	II1	120.2154	-9.5266	54.4 ± 0.5	4.2	760.1	18.97	53.62	0.68	6.33 ± 0.14
16-8	Profile 1	II2	120.2143	-9.5269	67.5 ± 0.5	4.5	774.6	6.49	55.51	0.47	4.45 ± 0.10
16-9	Profile 1	II3	120.2128	-9.5277	80.2 ± 0.5	4.0	797.7	8.81	55.37	0.31	4.8 ± 0.11
16-10	Profile 1	II4	120.2116	-9.5279	88.1 ± 0.5	3.1	811.6	2.89	55.14	0.15	5.53 ± 0.12
18-20	Profile 1	II4	120.2104	-9.5275	94.4 ± 0.5	3.6	816.7	1.75	52.58	0.40	13.17 ± 0.31
18-19	Profile 1	II5	120.2086	-9.5274	104.0 ± 0.5	3.3	831.3	3.67	53.59	0.28	9.54 ± 0.19
18-18	Profile 1	II6	120.2075	-9.5279	113.9 ± 0.5	3.6	847.2	2.47	52.72	0.36	7.63 ± 0.17
18-17	Profile 1	II6	120.2060	-9.5284	117.9 ± 0.5	1.5	867.0	4.32	52.75	0.34	11.47 ± 0.23
18-16	Profile 1	II7	120.2039	-9.5281	127.8 ± 0.5	3.6	881.6	5.57	47.47	0.42	13.57 ± 0.26
18-15	Profile 1	II7	120.2016	-9.5280	138.6 ± 0.5	8.2	901.0	3.16	50.46	0.30	3.80 ± 0.08
18-14	Profile 1	III	120.2004	-9.5283	163.0 ± 0.5	6.0	913.9	2.16	54.33	0.24	7.20 ± 0.16
18-37	Profile 1	IV	120.1909	-9.5272	227.1 ± 0.5	6.2	987.1	4.42	51.70		20.00 ± 0.37
18-36	Profile 1	V	120.1822	-9.5266	309.5 ± 1.5	7.3	1059.6	2.87	52.19	0.20	4.04 ± 0.09
18-35	Profile 1	V	120.1777	-9.5256	327.2 ± 1.5	8.8	1073.7	2.23	53.19	0.25	8.50 ± 0.17
18-31	Profile 1	VI	120.1738	-9.5278	380.5 ± 1.5	3.5	1101.7	2.43	53.20	0.46	15.00 ± 0.28
18-33	Profile 1	VII	120.1646	-9.5275	471.6 ± 1.5	2.7	1109.8	4.06	51.42	0.20	8.01 ± 0.17
18-24	Profile 2	I1	120.2149	-9.5072	14.7 ± 0.5	14.4	765.6	38.37	52.12	0.51	7.26 ± 0.16
18-25	Profile 2	I2	120.2144	-9.5074	25.8 ± 0.5	3.1	767.4	7.37	52.29	0.29	3.68 ± 0.08
18-26	Profile 2	II0	120.2132	-9.5075	35.2 ± 0.5	7.0	774.4	49.08	51.88	0.63	8.31 ± 0.21
18-28	Profile 2	II1	120.2123	-9.5075	43.3 ± 0.5	10.6	779.6	3.96	53.32	0.50	5.11 ± 0.11
18-27	Profile 2	II1	120.2118	-9.5076	56.1 ± 0.5	12.1	782.4	9.24	51.62	0.29	5.11 ± 0.11
Cmsurface	Borehole	I1	120.2237	-9.5336	2.8 ± 0.5	0.0	790.6	12.26	56.61	0.36	6.23 ± 0.14
Cm2.5m	Borehole	I1	120.2237	-9.5336	-2.5 ± 0.1			18.15	52.49	0.75	2.46 ± 0.06
18-46	Off profile	I1	120.2207	-9.5179	2.0 ± 0.5	0.0	638.9	245.15	47.14	2.67	0.38 ± 0.04
18-47	Off profile	I0	120.2207	-9.5179	0.0	0.0	638.9	178.84	49.93	1.43	0.30 ± 0.03
11-6	Off profile	II6	120.2009	-9.5217	149.3 ± 0.5	2.1	830.8	3.38	55.33	0.38	10.82 ± 0.23
14-2	Off profile	IV	120.1139	-9.5274	210.8 ± 0.5	3.5	1094.4	2.22	55.33	0.26	7.07 ± 0.15
14-2	Off profile	V	120.1141	-9.5407	293.9 ± 1.5	3.4	1142.8	1.97	55.69	0.14	8.27 ± 0.18

1330 **Table 2.** Bedrock sample information, location, elevation, chemical composition, and AMS ³⁶Cl results. Mean annual precipitation
1331 (MAP) values are TRMM data (e.g., Kummerow et al., 2000).

Sample (SUM)	Morphology location	AMS result [³⁶ C] (10 ⁹ atom g ⁻¹)	Hypothesis 1			Hypothesis 2			Hypothesis 3			Mean denudation rate (mm ka ⁻¹)	Integration time (ka)
			MIS	Exposure duration (ka)	Denudation rate (mm ka ⁻¹)	MIS	Exposure duration (ka)	Denudation rate (mm ka ⁻¹)	MIS	Exposure duration (ka)	Denudation rate (mm ka ⁻¹)		
16-1	Terrace main surface	5.95 ± 0.14	5a	82 ± 3	11.3 ± 0.1	5c	100 ± 5	13.7 ± 0.1	5e	122 ± 6	16.2 ± 0.1	13.7 ± 2.5	44.7 ± 8.0
16-2	Terrace main surface	5.43 ± 0.13	5a	82 ± 3	12.1 ± 0.1	5c	100 ± 5	14.4 ± 0.1	5e	122 ± 6	18.4 ± 0.1	15.0 ± 3.2	41.2 ± 8.5
18-22	Terrace main surface	4.82 ± 0.11	5a	82 ± 3	12.8 ± 0.4	5c	100 ± 5	175.1 ± 0.4	5e	122 ± 6	16.9 ± 0.4	14.9 ± 2.1	40.7 ± 5.7
16-3	Terrace main surface	6.1 ± 0.14	5a	82 ± 3	10.0 ± 0.1	5c	100 ± 5	12.5 ± 0.1	5e	122 ± 6	14.4 ± 0.1	12.3 ± 2.2	49.9 ± 9.3
18-21	Terrace main surface	4.69 ± 0.10	5a	82 ± 3	13.0 ± 0.4	5c	100 ± 5	15.2 ± 0.4	5e	122 ± 6	17.1 ± 0.4	15.1 ± 2.1	40.3 ± 5.7
16-4	Terrace main surface	6.26 ± 0.14	5a	82 ± 3	8.9 ± 0.1	5c	100 ± 5	11.3 ± 0.1	5e	122 ± 6	13.1 ± 0.1	11.1 ± 2.1	55.5 ± 11.3
16-6	Inner edge	9.7 ± 0.22	5e	122 ± 6	3.4 ± 0.0(2)	7e	239.5 ± 8.5	7.6 ± 0.0(2)				5.5 ± 2.9	127.9 ± 68.6
11-5	Distal edge	6.33 ± 0.14	5e	122 ± 6	12.8 ± 0.1	7e	239.5 ± 8.5	16.7 ± 0.1				14.7 ± 2.8	41.6 ± 7.8
16-8	Terrace main surface	4.45 ± 0.10	7e	239.5 ± 8.5	28.4 ± 0.2	9e	325 ± 18.5	30.4 ± 0.2				29.4 ± 1.4	20.4 ± 1.0
16-9	Terrace main surface	4.8 ± 0.11	7e	239.5 ± 8.5	25.4 ± 0.2	9e	325 ± 18.5	27.3 ± 0.2				26.4 ± 1.3	22.8 ± 1.1
16-10	Terrace main surface	5.53 ± 0.12	7e	239.5 ± 8.5	20.4 ± 0.1	9e	325 ± 18.5	22.1 ± 0.1				21.3 ± 1.2	28.3 ± 1.6
18-20	Terrace main surface	13.17 ± 0.31	7e	239.5 ± 8.5	3.4 ± 0.1	9e	325 ± 18.5	4.4 ± 0.1				3.9 ± 0.7	156.0 ± 26.8
18-19	Inner edge	9.54 ± 0.19	7e	239.5 ± 8.5	7.4 ± 0.2	9e	325 ± 18.5	8.3 ± 0.2				7.8 ± 0.7	76.8 ± 6.4
18-18	Distal edge	7.63 ± 0.17	9e	325 ± 18.5	11.6 ± 0.3							11.6 ± 0.3	51.7 ± 0.1
18-17	Terrace main surface	11.47 ± 0.23	9e	325 ± 18.5	6.0 ± 0.1							6.0 ± 0.1	99.5 ± 0.1
18-16	Terrace main surface	13.57 ± 0.26	9e	325 ± 18.5	3.6 ± 0.1							3.6 ± 0.1	164.8 ± 0.1
18-15	Inner edge	3.80 ± 0.08	9e	325 ± 18.5	31.3 ± 0.8							31.3 ± 0.8	19.2 ± 0.1
18-14	Distal edge	7.20 ± 0.16	9e	325 ± 18.5	13.8 ± 0.4	11c	390 ± 30	14.4 ± 0.4				14.1 ± 0.4	42.5 ± 1.4
18-37	Terrace main surface	20.00 ± 0.37	11c	390 ± 30	2.3 ± 0.1	13a	495 ± 15	2.8 ± 0.1				2.5 ± 0.3	237.3 ± 27.0
18-36	Distal edge	4.04 ± 0.09	15e	610 ± 10	37.0 ± 0.9	17c	695 ± 15	37.1 ± 0.9				37.1 ± 0.1	16.2 ± 0.3
18-35	Terrace main surface	8.50 ± 0.17	15e	610 ± 10	14.3 ± 0.3	17c	685 ± 15	14.4 ± 0.3				14.4 ± 0.1	41.8 ± 0.3
18-31	Inner edge	15.00 ± 0.28	19	780 ± 10	6.4 ± 0.1	21	850 ± 15	6.5 ± 0.1	23	910 ± 10	6.6 ± 0.1	6.5 ± 0.1	92.4 ± 0.8
18-33	Terrace main surface	8.01 ± 0.17	27	980 ± 5	17.1 ± 0.4	29	1020 ± 10	17.2 ± 0.4				17.2 ± 0.0(1)	35.0 ± 0.1
18-24	Inner edge	7.26 ± 0.16	5a	82 ± 3	6.1 ± 0.2	5c	100 ± 5	8.9 ± 0.2	5e	122 ± 6	10.8 ± 0.2	8.6 ± 2.4	73.8 ± 22.1
18-25	Distal edge	3.68 ± 0.08	5a	82 ± 3	19.7 ± 0.5	5c	100 ± 5	22.0 ± 0.5	5e	122 ± 6	24.0 ± 0.2	21.9 ± 2.2	27.6 ± 2.8
18-26	Terrace main surface	8.31 ± 0.21	5e	122 ± 6	9.4 ± 0.2	7e	239.5 ± 8.5	13.0 ± 0.2				11.2 ± 2.6	55.1 ± 12.8
18-28	Inner edge	5.11 ± 0.11	5e	122 ± 6	14.4 ± 0.4	7e	239.5 ± 8.5	19.0 ± 0.4				16.7 ± 3.3	36.6 ± 7.1
18-27	Distal edge	5.11 ± 0.11	5e	122 ± 6	17.8 ± 0.5	7e	239.5 ± 8.5	22.8 ± 0.5				20.3 ± 3.5	30.0 ± 5.3
18-46	Distal edge	0.38 ± 0.04	Holocene	2.13 ± 0.01	279.0 ± 0.4	Holocene	5.45 ± 0.02	581.0 ± 0.4				430 ± 214	1.6 ± 2.8
11-6	Inner edge	10.82 ± 0.23	9e	325 ± 18.5	8.4 ± 0.2							8.4 ± 0.2	71.4 ± 0.1
14-1	Terrace main surface	7.07 ± 0.15	11c	390 ± 30	16.8 ± 0.4	13a	495 ± 15	17.5 ± 0.4				17.1 ± 0.5	35.0 ± 1.1
14-2	Inner edge	8.27 ± 0.18	15e	610 ± 10	16.1 ± 0.4	17c	685 ± 15	16.3 ± 0.4				16.2 ± 0.1	37.0 ± 0.3

1332

1333 **Table 3.** Morphology location and calculated denudation rates from the ^{36}Cl concentrations and the different MIS and age hypotheses,
1334 assuming that the ages of reefal bioconstruction and exposure duration are synchronous, for each CRT of the sequence as proposed
1335 by Pirazzoli et al. (1991; 1993). The MIS ages and their uncertainties are derived from Cutler et al. (2003) and Murray-Wallace and
1336 Woodroffe (2014). Denudation rate uncertainties are calculated by standard error propagation, including uncertainties from production
1337 rates, ages, and AMS measurements. Mean denudation rate uncertainties are calculated using the standard deviation.

Porosity %	Density (g cm ⁻³)	Ed		Denudation rate (mm ka ⁻¹)	Ct2.5m (10 ⁵ atoms g rock ⁻¹)	Δc (10 ⁵ atoms g rock ⁻¹)	Ed Δc ka
		MIS	ka				
50	1.25	5a	82 ± 3	20.0 ± 0.2	1.88 ± 0.03	0.58 ± 0.15	5.4 ± 1.3
		5c	100 ± 5	24.9 ± 0.2	2.02 ± 0.03	0.44 ± 0.15	4.0 ± 1.2
		5e	122 ± 6	28.6 ± 0.3	2.18 ± 0.03	0.28 ± 0.15	2.6 ± 1.2
0	2.5	5a	82 ± 3	9.5 ± 0.2	1.05 ± 0.03	1.41 ± 0.15	13.8 ± 1.3
		5c	100 ± 5	11.9 ± 0.2	1.19 ± 0.03	1.27 ± 0.15	12.5 ± 1.2
		5e	122 ± 6	13.8 ± 0.3	1.34 ± 0.03	1.15 ± 0.15	11.0 ± 1.2

1338 **Table 4.** Borehole ³⁶Cl theoretical concentrations and theoretical exposure duration within CRT I₁. Ed, MIS, Ct2.5m, Δc , Ed Δc ,
1339 correspond to the exposure duration for surface sample (Cmsurface), Marine Isotope Stage, ³⁶Cl theoretical concentration at 2.5 ±
1340 0.1 m depth (Ct2.5m) calculated from the ³⁶Cl measured concentration of the surface sample, the difference between ³⁶Cl measured
1341 (Cm2.5m) and theoretical concentrations at 2.5 ± 0.1 m depth (Ct2.5m), the theoretical exposure duration calculated from Δc ,
1342 respectively. The ages and their uncertainties are derived from Cutler et al. (2003) and Murray-Wallace and Woodroffe (2014).